Session 0A4
Electromagnetic Near Field Effects in Problems of Wave Radiation from and Scattering by Ordered and Disordered Media

A Doppler Method to Measure Forward Scattering of Radiowaves at Near Grazing Angles

G. Koh and S. A. Arcone
U. S. Army ERDC-CRREL, USA

We are developing a Doppler method to measure bistatic forward and backscatter from rough surfaces on a rotating table. The method avoids interference between the forward scatter and the direct signal between antennas. We use a 90-GHz FMCW system converted for Doppler use. We use horn lens antennas to produce a 1.4 degree beamwidth that illuminates a small area of the rotating table within which the translational velocity is fairly uniform; a more exact calculation of velocity variations within the area has not yet been worked out. The table rotates at about 0.05 Hz, which provides a translational velocity of about 0.3 m/s within the illuminated area and a Doppler shift of about 75 Hz. We rectify our measured signal and form our scattering probability density functions from the peak amplitudes, of which about 1500 occur during one table rotation. Our minimum grazing angle is still a relatively large 10 degrees. However, this limitation is imposed only by blockage of the antenna aperture by the edge of the one-meter radius table; smaller angles could be achieved with a larger table. Preliminary results for very rough scattering by crushed rock of 0.5–2 cm size show Rayleigh distributions for backscatter with a greater concentration of higher amplitudes at the smaller incidence angles of 60–70 degrees. The forward scatter shows more Gaussian distributions with greater amplitudes occurring at 75–80 degrees. These general results are expected. Rms heights and autocorrelation functions of the surfaces were measured on a separate, stationary surface with a laser profilometer, but this instrument could easily be adapted to a stationary mode over the rotating table. Calibration of absolute reflectivity will require a flat plate and precise beam alignments, and a more careful description of the illumination pattern is needed because the table is not in the far field.

Extended Unitarity for S-matrix and Electromagnetic Radiation Transfer in Dielectric Random Media with Effects of Near Fields and Opposite Wave Streams' Interference

Y. N. Barabanenkov and M. Y. Barabanenkov
Russian Academy of Sciences, Russia

The phenomenological radiative transfer theory is derived from the theory of wave multiple scattering in random media at neglecting the repeated scattering of a monochromatic wave by just the same inhomogeneity— so-called single-group approximation, together with the far-field approximation for fields scattered by inhomogeneities [1]. The best-known effect of the multi-group scattering events is the coherent backscattering enhancement (weak localization) caused by the contribution of so-called cyclical (maximally crossed) diagrams [2]. This effect gives a correction to the transfer equation for backward scattering cone, with cone width being of the order of the wavelength over the extinction length [3]. Despite the achivements of the weak localization theory, there is a problem to conform the contribution of the maximally crossed diagrams into multiple scattering of waves to the energy conservation law.

In this report we present an original and perhaps unexpected resolution to the stated problem using a physical idea that the weak localization phenomenon should be coupled with the evanescent waves in a random medium. Technically our approach is based on the modern development of the wave multiple scattering theory in terms of Sommerfeld-Weyl angular-spectrum decomposition of wave amplitudes, transfer relations [4], extended unitarity for 2×2 block S-scattering matrix and effect of energy emission from an evanescent wave [5]. In result we derive a transfer equation for 2×2 block coherence matrix of angular-spectrum amplitudes of waves inside a 3D random medium slab. The diagonal blocks of the coherence matrix describe the autocoherence peculiarities of waves going forward or backward with respect to an embedding parameter into the medium slab but the off-dioganal blocks present the cross-coherence of the opposite going waves. The derived transfer equation possesses a specific energy invariant (pseudo-trace of the coherence matrix), in respect of the embedding parameter, that conforms its solution to the energy coservation law, the energy transformation between propagating and evanescent waves being taken into account. We evaluate with the aid of this transfer equation a relative contribution of evanescent waves into the coherent backscattering of waves; the influence of evanescent waves on coherent backscattering cone width and on reducing of the random medium depth where the coherent backscattering is actually formed; a specific dependence of the evanescent waves' effect on the shape of a random medium inhomogeneity.

REFERENCES

1. Barabanenkov, Y. N. and V. M. Finkelberg, *Sov. Phys. JETP*, Vol. 26, 587–591, 1968.
2. Barabanenkov, Y. N., Y. A. Kravtsov, V. D. Ozrin, and A. I. Saichev, "Enhanced backscattering in optics," *Progress in Optics*, ed. Wolf, E., Elsevier, Amsterdam, Vol. 29, 65–197, 1991.
3. Barabanenkov, Y. N., "Wave corrections to the transport equation for backscattering," *Izv. Vyssch. Uchebn. Zaved. Radiofiz.*, Vol. 16, 88–96, 1973.
4. Barabanenkov, Y. N., V. L. Kouznetsov, and M. Y. Barabanenkov, *Progress in Electromagnetic Research, PIER*, ed. Kong, J. A., EMW, Cambridge, England, Vol. 24, 39–75, 1999.
5. Gulyaev, Y. V., Y. N. Barabanenkov, M. Y. Barabanenkov, and S. A. Nikitov, *Phys. Lett. A*, Vol. 335, 471–472, 2005; *Phys. Rev. E*, Vol. 72, 026602-1-026602-12, 2005.

Energy Invariants to Composition Rules for Scattering and Transfer Matrices of Propagating and Evanescent Waves in Dielectric Structures

Y. N. Barabanenkov
Institute of Radioengineering and Electronics of Russian Academy of Sciences, Russia

M. Y. Barabanenkov
Institute of Microelectronics Technology and High Purity Materials of Russian Academy of Sciences, Russia

Abstract—We present as a basis to modern wave multiple scettering theory an extended unitarity for the S-scattering matrix and an extended pseudo-unitarity for the transfer matrix of propagating and evanescent (near field) electromagnetic waves in a volume or surface lossless dielectric structure with spatial inhomogeneities of any dimension. The formalism of angular spectrum wave amplitudes is used. The presented extended unitarity and pseudo-unitarity are shown to be energy invariants to composition rules for the S-matrix and the transfer matrix,respectively. From composition rules, we derive a complete system of nonlinear differential equations for blocks of the S-matrix, with Riccati equation being a main one, and a linear equation for the transfer matrix.

Section 1.

During the last one and half decade the wave multiple scattering theory based on composition rule [1] for scattering operator (T-matrix) was reformulated in terms of virtual splitting the volume or surface inhomogeneous dielectric structure into a stack of elementary layers (slices), with slices being perpendicular to an embedding parameter and separated by splits, which may be vanishingly thin. In result using the Sommerfeld-Weyl angular-spectrum decomposition of wave amplitudes, a system of exact equations (transfer relation) [2] was obtained for the operator wave reflection and transmission coefficients of the structure and the operator wave amplitudes of waves in splits between slices (local fields).

The report aims to show that the recently derived, at study the effect of energy emission from an evanescent wave, extended unitarity of the 2×2 block S-scattering matrix [3] is an energy invariant to a specific composition rule for S-matrix, which is a consequence from the transfer relations. This composition rule describes the incremental change of S-matrix of subsystem of slices upon attachment an additional subsystem of slices. In the case of infinitesimally thin attached slice, we obtain a complete system of nonlinear differential equations for blocks of the S-matrix, with Riccati equation being a main one and taking into account a strong singularity of the electric field Green tensor function in a background. The S-matrix is closely related to the transfer matrix, for which we derive a linear equation with an energy invariant in the form of an extended pseudo-unitarity of the transfer matrix.

Section 2.

Let a volume or surface dielectric structure with scalar dielectric permittivity $\epsilon(\vec{r})$ occupies a region between planes $z=0$ and $z=L$ of Cartesian coordinate system x, y, z. The electric field of monochromatic electromagnetic wave to be incident onto the left boundary plane $z=0$ is written as (see details in [2] and [3]) $(2\pi)^{-2}\int d\vec{k}_\perp \exp(i\vec{k}_\perp\vec{r}_\perp)E^\circ_\alpha(\vec{k}_\perp)\exp(i\gamma_k z)$. Here $\vec{k}_\perp$ is the transverse to the z axis component of a wave vector $\vec{k}$, and the angular spectrum amplitude $E^\circ_\alpha(\vec{k}_\perp)$ of the incident electric field describes either propagating or evanescent wave, depending on $k_\perp < k_\circ$ and $\gamma_k=\sqrt{k_\circ^2-k_\perp^2}$ is real or $k_\perp > k_\circ$ and $\gamma_k = i\sqrt{k_\perp^2-k_\circ^2}$ is purely imaginary quantity, respectively. The quantity $k_\circ$ is the wave number in a background with dielectric permittivity $\epsilon_\circ$. The angular spectrum amplitudes of electric field, transmitted through and reflected from the structure, are written in terms of the tensor operator transmission $A_{\alpha\beta}(\vec{k}_\perp,\vec{k'}_\perp)$ and reflection $B_{\alpha\beta}(\vec{k}_\perp,\vec{k'}_\perp)$ coefficients of plane wave, which may be evanescent, as $(2\pi)^{-2}\int d\vec{k}_\perp A_{\alpha\beta}(\vec{k}_\perp,\vec{k'}_\perp)E^\circ_\beta(\vec{k'}_\perp)$ and $(2\pi)^{-2}\int d\vec{k}_\perp B_{\alpha\beta}(\vec{k}_\perp,\vec{k'}_\perp)E^\circ_\beta(\vec{k'}_\perp)$, respectively. An electromagnetic wave may be incident upon the right boundary plane $z=L$ with angular spectrum amplitude $\tilde{E}^\circ_\alpha(\vec{k}_\perp)$. In this case the angular spectrum amplitudes of electric field, transmitted through and reflected from the structure, are written in terms of the tensor operator transmission $\tilde{A}_{\alpha\beta}(\vec{k}_\perp,\vec{k'}_\perp)$ and reflection $\tilde{B}_{\alpha\beta}(\vec{k}_\perp,\vec{k'}_\perp)$ coefficients of plane wave.

The 2×2 block S-matrix of the structure is defined in terms of the above tensor coefficients of wave transmission through and reflection from structure as follows

$$S = \begin{pmatrix} A & \tilde{B} \\ B & \tilde{A} \end{pmatrix} \tag{1}$$

Physically the S-matrix transforms the angular spectrum amplitudes of incident forward and backward going waves, with respect to positive direction of the z axis,into the angular spectrum amplitudes of scattered forward and backward going waves.

Section 3.

Split virtually the dielectric structure under consideration into a stack of n slices with splits between them, as in Fig. 1 of [2]. According to this reference, the composition rule [1] for the scattering operator (T-matrix) together with condition of non-overlapping the slices lead to a mixed system of exact equations-transfer relations for blocks of the S-matrices of subsystems of slices and amplitudes of local waves inside splits. As doing so the tensor coefficients of the local fields waves in splits can be eliminated from the transfer relations and expressed in terms of blocks of the S-matrices, $S_{1,m}$ and $S_{m+1,n}$. After this elimination, the transfer relations give the separate system of recurrent equations that describes the incremental change of the S-matrix of subsystem of slices with numbers $1,\ldots,m$ upon attachment of additional subsystem of slices with numbers $m+1,\ldots,n$. This system of recurrent equations has been got in [2] for the case of 2D dielectric structure and TE polarization, with $m = n-1$, and for general case has a form

$$\begin{aligned} A_{1,n} &= A_{m+1,n}(I - \tilde{B}_{1,m}B_{m+1,n})^{-1}A_{1,m}, \\ B_{1,n} &= B_{1,m} + \tilde{A}_{1,m}B_{m+1,n}(I - \tilde{B}_{1,m}B_{m+1,n})^{-1}A_{1,m} \end{aligned} \tag{2}$$

and

$$\begin{aligned} \tilde{A}_{1,n} &= \tilde{A}_{1,m}(\tilde{I} - B_{m+1,n}\tilde{B}_{1,m})^{-1}\tilde{A}_{m+1,n}, \\ \tilde{B}_{1,n} &= \tilde{B}_{m+1,n} + A_{m+1,n}\tilde{B}_{1,m}(\tilde{I} - B_{m+1,n}\tilde{B}_{1,m})^{-1}\tilde{A}_{m+1,n} \end{aligned} \tag{3}$$

The symbols I and $\tilde{I}$ denote some identity tensor operators, $I_{\alpha\beta}(\vec{k}_\perp, \vec{k'}_\perp) = P^{tr}_{\alpha\beta}(\hat{k}^+)\delta_{\vec{k}_\perp,\vec{k'}_\perp}$ and $\tilde{I}_{\alpha\beta}(\vec{k}_\perp, \vec{k'}_\perp) = P^{tr}_{\alpha\beta}(\hat{k}^-)\delta_{\vec{k}_\perp,\vec{k'}_\perp}$, acting in the subspaces of transverse inhomogeneous plane waves going forward and backward with the wave vectors $\vec{k}^\pm = \vec{k}_\perp \pm \gamma_k\hat{z}$, respectively, where $\hat{z}$ is the unit vector along the z axis. Besides, the units vectors along these wave vectors are defined by, $\hat{k}^\pm = \hat{k}^\pm/k_\circ$, and a tensor, $P^{tr}_{\alpha\beta}(\hat{k})$, means the orthogonal projector in direction perpendicular to the unit vector $\hat{k}$. One should note here that in the scalar case a system of recurrent equations similar to Eqs. (2, 3) has been got by Redheffer [4] as the functional relations (semigroup property) associated with the Riccati system of equations for the reflection and transmission coefficients of waves propagating in transmission lines. In this case, Regheffer has introduced an useful notion *star product*, (*), of the scattering matrices, which enables us to rewrite the above system of reccurrent Eqs. (2, 3) shortly as $S_{1,n} = S_{1,m} * S_{m+1,n}$.

Section 4.

Turn to the composition rule for S-matrix in Eqs. (2, 3) and consider the case of thin attached nth slice, $m = n-1$. We introduce a useful renormalized version $\mathbf{S}$ of the scattering matrix (1) putting $\boldsymbol{S} = \mathrm{diag}(\gamma^{1/2}, \gamma^{1/2})S$ $\mathrm{diag}(\gamma^{-1/2}, \gamma^{-1/2})$ and suppose the S-matrix of the nth slice to be small deviated from an identity matrix, $\mathbf{I}=\mathrm{diag}(I, \tilde{I})$, and subject to a condition, $\mathbf{S_{n,n}} = \mathbf{I} + \delta\mathbf{S}\Delta\mathbf{z}$. Here a thickness Δz of the nth slice tends to zero and an infinitesimal scattering matrix δS is obtained by a solution to the Lippman-Schwinger equation for T-matrix in the form

$$\delta\mathbf{S} = \begin{pmatrix} \mathbf{U}^{++} & \mathbf{U}^{+-} \\ \mathbf{U}^{-+} & \mathbf{U}^{--} \end{pmatrix} \tag{4}$$

The blocks of this infinitesimal scattering matrix are given by

$$\mathbf{U}^{\xi\eta}_{\alpha\beta}(\vec{k}_\perp, \vec{k'}_\perp; z) = \frac{1}{2i}\exp[-i(\xi\gamma_k - \eta\gamma_{k'})z]\frac{1}{\sqrt{\gamma_k}}U^{\xi\eta}_{\alpha\beta}(\vec{k}_\perp, \vec{k'}_\perp; z)\frac{1}{\sqrt{\gamma_{k'}}} \tag{5}$$

with

$$\begin{aligned} U^{\xi\eta}_{\alpha\beta}(\vec{k}_\perp, \vec{k'}_\perp; z) &= P^{tr}_{\alpha\mu}(\hat{k}^\xi)U_{\mu\nu}(\vec{k}_\perp - \vec{k'}_\perp, z)P^{tr}_{\nu\beta}(\hat{k}^{\eta'}) \\ U_{\alpha\beta}(\vec{k}_\perp, z) &= V(\vec{k}_\perp, z)(\hat{x}_\alpha\hat{x}_\beta + \hat{y}_\alpha\hat{y}_\beta) + v(\vec{k}_\perp, z)\hat{z}_\alpha\hat{z}_\beta \end{aligned}$$

where $\xi, \eta = \pm$, $V(\vec{k}_\perp, z)$ and $v(\vec{k}_\perp, z)$ are the spatial Fourier transforms of the scalar potential $V(\vec{r}) = -k_\circ^2[\epsilon(\vec{r}) - \epsilon_\circ]/\epsilon_\circ$ and a function $v(\vec{r}) = -k_\circ^2[\epsilon(\vec{r}) - \epsilon_\circ]/\epsilon(\vec{r})$, respectively, with respect to transverse to the z axis component of the position vector, $\hat{x}$ and $\hat{y}$ are unit vectors along the x and y axes, respectively. Substituting the obtained asymptotics for the S-matrix of thin nth slice into composition rule in Eqs. (2), (3) gives the following systems of differential equations for blocks of the $\mathbf{S}$-matrix

$$\frac{d\tilde{\mathbf{B}}}{dz} = \mathbf{U}^{+-} + \mathbf{U}^{++}\tilde{\mathbf{B}} + \tilde{\mathbf{B}}\mathbf{U}^{--} + \tilde{\mathbf{B}}\mathbf{U}^{-+}\tilde{\mathbf{B}}, \qquad \tilde{\mathbf{B}}(z=\mathbf{0}) = \mathbf{0} \tag{6}$$

$$\frac{d\tilde{\mathbf{A}}}{dz} = \tilde{\mathbf{A}}(\mathbf{U}^{--} + \mathbf{U}^{-+}\tilde{\mathbf{B}}), \qquad \tilde{\mathbf{A}}(z=0) = \tilde{I} \tag{7}$$

$$\frac{d\mathbf{A}}{dz} = (\tilde{\mathbf{B}}\mathbf{U}^{-+} + \mathbf{U}^{++})\mathbf{A}, \qquad \mathbf{A}(z=\mathbf{0}) = I \tag{8}$$

$$\frac{d\mathbf{B}}{dz} = \tilde{\mathbf{A}}\mathbf{U}^{-+}\mathbf{A}, \qquad \mathbf{B}(z=\mathbf{0}) = \mathbf{0} \tag{9}$$

Klyatskin [5] derived a matrix Riccati equation similar to Eq. (6) in scalar case.

Section 5.

By straightforward calculation, one can verify that the infinitesimal scattering matrix (4) satisfies the following extended unitarity condition

$$(\mathbf{H}^{pr} + i\mathbf{H}^{ev}\Sigma_x)\delta\mathbf{S} + [(\mathbf{H}^{pr} + i\mathbf{H}^{ev}\Sigma_x)\delta\mathbf{S}]^\dagger = 0 \tag{10}$$

where $\mathbf{H}^{pr}$ and $\mathbf{H}^{ev}$ denote projectors on propagating and evanescent waves, respectively, and $\Sigma_x = \left(\begin{smallmatrix} 0 & 1 \\ 1 & 0 \end{smallmatrix}\right)$ is a block Pauli matrix (see [3]). On the other hand, one can also prove that the *star product* of two S-matrices does satisfies the extended unitarity from [3] in the form

$$(\mathbf{H}^{pr}\mathbf{S})^\dagger(\mathbf{H}^{pr}\mathbf{S}) = \mathbf{H}^{pr}\mathbf{I}\mathbf{H}^{pr} - i[\mathbf{H}^{ev}\Sigma_x\mathbf{S} - (\mathbf{H}^{ev}\Sigma_x\mathbf{S})^\dagger] \tag{11}$$

if the both S-matrices satisfy (11) separately. Bearing in mind that the *star product* is associative [4], we conclude that a solution to the derived Riccati system of equations satisfies the extended unitarity (11).

Section 6.

The transfer matrix $\mathbf{M}$ transforms, in different from the $\mathbf{S}$-matrix, the angular spectrum amplitudes of forward and backward going waves on the left side of the structure into ones on the right side of the structure. This definition gives the known relation between matrices under consideration (see, e. g., [2]) and leads from the derived Riccati-system of equations to the following linear differential equation for the transfer matrix

$$\frac{d\mathbf{M}}{dz} = \Sigma_z\delta\mathbf{S}\mathbf{M}, \qquad \mathbf{M}(z=0) = \mathbf{I} \tag{12}$$

were $\Sigma_z = \left(\begin{smallmatrix} 1 & 0 \\ 0 & -1 \end{smallmatrix}\right)$ is a block Pauli matrix. Starting with the extended unitarity (10) for the infinitesimal scattering matrix one can verify by direct differentiation that a solution to the obtained linear equation has an energy invariat in a form of the following extended pseudu-nitarity for the transfer matrix

$$\mathbf{M}^\dagger\Sigma_z(\mathbf{H}^{pr} - i\Sigma_x\mathbf{H}^{ev})\mathbf{M} = \Sigma_z(\mathbf{H}^{pr} - i\Sigma_x\mathbf{H}^{ev}) \tag{13}$$

This extended pseudu-unitarity for the transfer matrix generalizes the known pseudu-unitarity constraint [6] on the case when evanescent waves may be present.

7. Conclusion

Summarizing, the presented complete system of differential equations for blocks of the S-matrix and differential equation for the transfer matrix together with their energy invariants can be considered as an analytical basis to incorporate the modern theory of electromagnetic wave multiple scattering by dielectric structures with near field effects.

REFERENCES

1. Goldberger, M. L. and K. M. Watson, *Collision Theory*, Wiley, New York, 1964.
2. Barabanenkov, Y. N., V. L. Kouznetsov, and M. Y. Barabanenkov, *Progress in Electromagnetic Research, PIER*, Ed. by J. A. Kong (EMW, Cambridge, 1999), Vol. 24, 39; *J. Electrmagn. Waves A*, Vol. 13, 1335, 1999.
3. Gulyaev, Y. V., Y. N. Barabanenkov, M. Y. Barabanenkov, and S. A. Nikitov, *Phys. Rev. E.*, Vol. 72, 026602, 2005.
4. Redheffer, R., *J. Math. and Mech.*, Vol. 8, 349, 1959.
5. Klytskin, V. I., "The imbedding method in the theory of wave propagation," Nauka, Moscow, 1980, (in Russian).
6. Mello, P. A., P. A., P. Pereyra, and N. Kumar, *Annals of Physics*, Vol. 181, 290, 1988.

Near Fields in Electromagnetic Wave Multiple Scattering in Random Media

Y. N. Barabanenkov and M. Y. Barabanenkov
Russian Academy of Sciences, Russia

Usually the near fields are not taken into account in study the electromagnetic wave multiple scattering in random media. Nevertheless their effects may be substantial, as it is shown in this report, even in such coherent phenomena as weak localization of waves in random media. Besides a contribution of near fields may be strong dependent on the shape of random medium inhomogeneity. One should note that consistent consideration the near fields effects became possible after a modern development of the wave multiple scattering theory in terms of Sommerfeld-Weyl angular-spectrum decomposition of wave amplitudes, transfer relations [1] and extended unitarity for 2×2 block S-scattering matrix [2], with accounting for energy transformation between propagating and evanescent waves at scattering by dielectric structures.

We start with a system of equations for angular spectral amplitudes of local monochromatic field waves going forward and backward with respect to an embedding parameter into the 3D random medium slab with given boundary conditions on the slab boundaries. We write also the Liouville type equation for 2×2 block density matrix of angular spectral amplitudes. This Liouvile equation possesses a specific energy invariant (pseudo-trace of density matrix), with respect to the embedding parameter. Applying the Furutsu-Dosker-Novikov formalism [3], we obtain the Dyson type equation in Bourret approximation for ensemble averaged angular spectral amplitudes and the transfer equation for 2×2 block coherence matrix. The Dyson equation is simple resolved, with result showing a strong dependence of evanescent wave contribution into coherent reflectance from slab on shape of dielectric permittivity correlation function. The transfer equation is transformed to integral form which can be resolved by iteration procedure. Every term of this procedure includes, in particular, products of opposite going waves' spectral amplitudes which may be propagating or evanescent, that gives a possibility to evaluate a relative contribution of evanescent waves into the coherent backscattering of waves and the influence of evanescent waves on coherent backscattering cone width and on reducing of the random medium depth where the coherent backscattering is actually formed.

REFERENCES

1. Barabanenkov, Y. N., V. L. Kouznetsov, and M. Y. Barabanenkov, *Progress in Electromagnetic Research, PIER*, ed. Kong, J. A., EMW, Cambridge, England, Vol. 24, 39–75, 1999.
2. Gulyaev, Y. V., Y. N. Barabanenkov, M. Y. Barabanenkov, and S. A. Nikitov, *Phys. Rev. E*, Vol. 72, 026602-1-026602-12, 2005.
3. Rytov, S. M., Y. A. Kravtsov, and V. I. Tatarskii, *Principles of Statistical Radiophisics*, Vol. 3, *Wave Propagation through Random Media*, Springer, Berlin, 1989.

Local Dielectric Measurement by Waveguide-type Microscopic Aperture Probe

T. Suzuki, **K. Sugimoto**, **Y. Yamagami**, **T. Negishi**, **and Y. Watanabe**
Nippon Institute of Technology, Japan

Abstract—For dielectric constant measurement of areas smaller than the wavelength, this paper proposes a method of employing waveguide-type microscopic aperture probe. The probe is made of WR-15 waveguide with one end shielded with metal plate of 0.3 mm, on which a 0.5 mm-dia or a 0.1 mm-dia aperture is made. The dielectric constant is derived from the slope of phase difference swept over 50–70 GHz between the cases of free-space transmission with and without the dielectrics. In order to evaluate the system, the dielectric constant of Teflon has been measured by three cases of using the probes of 0.5 mm-dia and 0.1 mm-dia, and two V-band corrugated horns. The results show good agreement.

1. Introduction

One of the well-established dielectric measurement methods in millimeter and submillimeter wave bands is the free-space transmission method using two horns[1]. That is sufficient for large objects compared to the wavelength. For the measurement of microscopic regional dielectric distribution of heterogeneous dielectric materials and cellular tissues, the aperture must be downsized so as the spatial resolution to be smaller than the wavelength [2].

As the embodiment of small aperture, waveguide-type probes are employed in this research. The probe is made of WR-15 waveguide with one end shielded with metal plate of 0.3 mm, on which a 0.5 mm-dia or a 0.1 mm-dia aperture is made. Figure 1 shows the outline. The probe replaces one horn at the transmission side in the free-space transmission measurement.

A microscopic aperture illuminates the region comparable to the aperture size, so that it realizes high spatial resolution of scanning microscopy for surface topography. Furthermore, employing the millimeter and submillimeter wavebands enables spectroscopic analysis, for example, oxygen content analysis by 60 GHz band as envisioned. On the other hand, it must be experimentally investigated to evaluate the decrease of the signal-to-noise ratio.

In order to evaluate the system, the dielectric constant of Teflon has been measured both by the proposed system and the free-space transmission method using two V-band corrugated horns with the aperture diameter 31 mm.

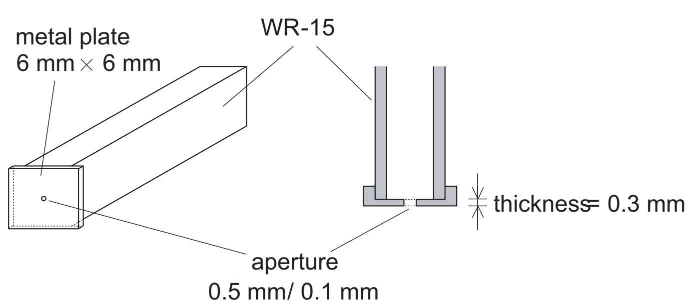

Figure 1: Waveguide-type probe.

2. Measurement

The dielectric constants is obtained from the slope of phase difference between the case of free-space transmission with and without the dielectrics. Relative dielectric constant ε_r is derived by

$$\varepsilon_r = (\frac{300\Delta\phi}{360d} + 1)^{\frac{1}{2}} \tag{1}$$

where $\Delta\phi$ (degree/GHz) is the slope of the phase difference, and d (mm) is the sample thickness. As a dielectric sample, a Teflon plate 100 mm × 100 mm × 4.1 mm (thickness) is used. The Teflon plate is contacted with the transmission side horn or the probe.

The phase difference is measured by using the vector network analyzer MVNA 8-350 (AB Millimeter, France). The lower frequency limit of the probe is determined by the cutoff frequency 40 GHz for the TE10 mode of WR-15. The frequency is swept over 50–70 GHz at 0.1 GHz step.

3. Result

The measurement of phase difference is made three times to obtain the average ε_r. One result by each system is shown in Figure 2. The solid line shows the measured phase difference, and the dotted line is derived by the least square method. As the aperture is smaller, the phase variance is increasing. The two-horn system gives $\varepsilon_r = 1.99$ and the proposed system gives $\varepsilon_r = 1.89$ with 0.5 mm aperture and $\varepsilon_r = 1.93$ with 0.1 mm aperture. They show good agreement, although the proposed systems have larger variance of phase difference.

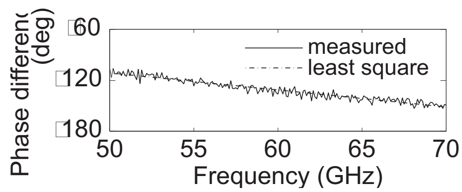

(a) Two-horn system.

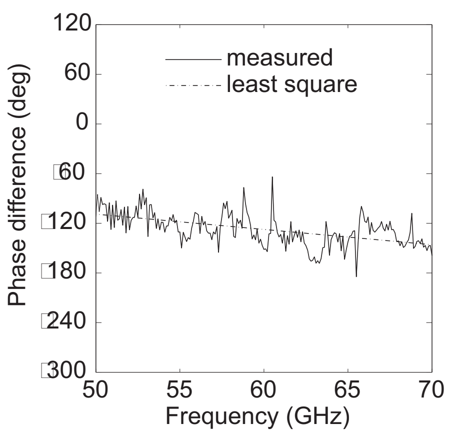

(b) Probe with 0.5 mm-dia aperture.

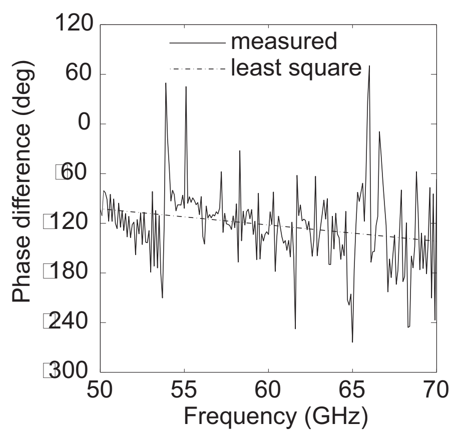

(c) Probe with 0.1 mm-dia aperture.

Figure 2: The phase difference and the slope measured by the two-horn free-space transmission method (a) and the proposed probes (b) and (c).

4. Conclusion

The dielectric constant has been measured by the waveguide-type microscopic aperture probes with 0.5 mm and 0.1 mm-dia, and the standard two-horn free-space transmission method as a reference. There is a good agreement between three results, while they show slightly small values compared to the nominal value of Teflon 2.1. The next step is the measurement by scanning with improved accuracy.

REFERENCES

1. Goy, P., and M. Gross, "Free-space vector transmission-reflection from 18 to 760 GHz," *24th European Microwave Conference*, Communication C10.5, France, September 1994.
2. Schade, U., K. Holldack, P. Kuske, and G. Wustefeld, "THz near-field imaging employing synchrotron radiation," *Applied Physics Letters*, Vol. 84, No. 8, 1422–1424, 2004.

Power Absorption of Near Field of Elementary Radiators in Proximity of a Composite Layer

M. Y. Koledintseva, **P. C. Ravva**, **J. Y. Huang**, **and J. L. Drewniak**
University of Missouri-Rolla, USA

M. Sabirov, **V. V. Bodrov**, **I. V. Sourkova**, **and V. I. Sourkov**
Moscow Power Engineering Institute (Technical University), Russia

Abstract—Near-field behavior of elementary electric and magnetic dipoles close to a plane layer (or layers) of engineered composite materials is analyzed using the rigorous analytical approach. Some results of computations are represented for composite media containing conductive inclusions. These composites provide shielding mainly due to absorption of electromagnetic energy. The effect of conductivity of inclusions and their geometry (through their aspect ratio) on the absorption and radiation efficiency of a radiator near composite layers is analyzed.

1. Introduction

The problems of studying electromagnetic interaction of different radiators with composite layered structures both in far- and near-field zones arise at the development of shielding enclosures for different electronic devices. In [1], the approach to engineering composites with the desired frequency response based on Maxwell Garnett (MG) formulation and a genetic algorithm is presented. An engineered infinitely large composite layer of finite thickness in [1] is considered for both normal and oblique incident plane waves. However, concepts of reflection and transmission coefficients, as well as of angles of incidence and polarization, are applicable only to the far-field region. In the near-field zone, it is better to consider field intensity attenuation due to such effects as excitation of evanescent waves, scattering, and different mechanisms of ohmic loss and energy transformation. In [2], the notions of absorption and radiation efficiencies in terms of power are introduced, and the corresponding power fluxes are calculated rigorously and explicitly via the spectra of the fields using the known solutions of boundary problems for parallel-plane, cylindrical, and spherical cases.

This paper considers the near-field behavior of elementary electric and magnetic dipoles close to a plane layer (or layers) of engineered composites, and the effect of conductivity of inclusions and their geometry (through the aspect ratio) on the absorption and radiation efficiency of a radiator near composite layers is studied.

2. Mathematical Model

2.1. Maxwell Garnett Formalism for Composites Containing Conductive Inclusions

The MG formulation is well-suited for modeling of linear electrodynamically isotropic multiphase mixtures of metallic or dielectric particles in a homogeneous dielectric base, where the parameters of the mixture do not change in time according to some law as a result of some external force—electrical, mechanical, etc.; inclusions are at the distances greater than their characteristic size; and the characteristic size of inclusions is small compared to the wavelength in the effective medium. The generalized MG mixing formula for multiphase mixtures with randomly oriented ellipsoidal inclusions is [1, 3],

$$\varepsilon_{eff} = \varepsilon_b + \frac{\frac{1}{3}\sum\limits_{i=1}^{n} f_i(\varepsilon_i - \varepsilon_b)\sum\limits_{k=1}^{3}\frac{\varepsilon_b}{\varepsilon_b + N_{ik}(\varepsilon_i - \varepsilon_b)}}{1 - \frac{1}{3}\sum\limits_{i=1}^{n} f_i(\varepsilon_i - \varepsilon_b)\sum\limits_{k=1}^{3}\frac{N_{ik}}{\varepsilon_b + N_{ik}(\varepsilon_i - \varepsilon_b)}} \tag{1}$$

where $\varepsilon_b(j\omega) = \varepsilon_{\infty b} + \chi_b(j\omega)$ and $\varepsilon_i(j\omega) = \varepsilon_{\infty i} + \chi_i(j\omega)$ are the relative permittivity of the base and of the i-th type of inclusions, respectively. In (1), f_i is the volume fraction occupied by the inclusions of the i-th type; N_{ik} are the depolarization factors [4] of the i-th type of inclusions, where indices $k = 1, 2, 3$ corresponds to x, y, and z coordinates. If the inclusions are thin cylinders, their two depolarization factors are close to $1/2$, and the third can be calculated as in [5], $N \approx (a)^{-2}\ln(a)$, where $a = l/d$ is a cylinder's aspect ratio (length/diameter). Since the MG formula is linear, the resultant effective permittivity of the mixture can be also represented through effective high-frequency permittivity and susceptibility function,

$$\varepsilon_{eff}(j\omega) = \varepsilon_{\infty eff} + \chi_{eff}(j\omega). \tag{2}$$

If inclusions are conducting (metallic), their frequency characteristic in terms of relative permittivity is

$$\varepsilon_i(j\omega) = \varepsilon' - j\varepsilon'' = \varepsilon' - j\sigma/\omega\varepsilon_0. \tag{3}$$

The MG rule is applicable when the concentration of the conducting particles is below the percolation threshold, $p_c \cong C/a \ll 1$, where a is an aspect (axis) ratio for the inclusions in the form of highly prolate spheroids [6], and C is the experimental coefficient depending on the composite morphology (typically, $C = 1-10$). Otherwise, the different approximations from the general effective medium theories should be used, for example, McLachlan [7] or Ghosh-Fuchs approximations [8].

The base material might be quite transparent over the frequency range where high shielding effectiveness is desirable. However, if there are conducting inclusions, the shielding effectiveness will be provided by absorption of electromagnetic energy due to conductivity loss and to the dimensional resonance in the particles. Presence of conductive particles will also increase reflection from the composite layer. In this paper, non-conductive composite materials (with dilute phase of conducting inclusions) are modeled. Non-conductive composites mainly absorb (rather than reflect) the energy of unwanted radiation. The effect of conductivity of inclusions and their geometry on the absorption and radiation efficiency of a radiator near composite layers is studied using the method described below.

2.2. Power Fluxes and Radiation and Absorption Efficiency in a Parallel-plane Structure

The near-field behavior of elementary radiators in proximity of a composite planar layer is studied using the unified rigorous analytical approach developed in [2, 9]. Herein, this approach is specified for the parallel-plane geometry. Power radiation efficiency and absorption efficiency are calculated, using formulas similar to those introduced in [2],

$$\eta_{rad} = 10\log_{10}[(P_{rad} - P_{loss})/P_{rad}] \text{ and } \eta_{abs} = 10\log_{10}[P_{loss}/P_{rad}]. \tag{4}$$

The radiated power P_{rad} and the power loss P_{los} are defined for a parallel-plane dielectric layer (see Figure 1):

$$P_{rad} = P_{Z1} + P_{Z2}; \quad P_{loss} = P_{Z1} - P_{Z3}. \tag{5}$$

The z-component of the Poynting vector in the parallel-plane geometry is

$$p_z = 0.5Re(E_x H_y^* - E_y H_x^*), \tag{6}$$

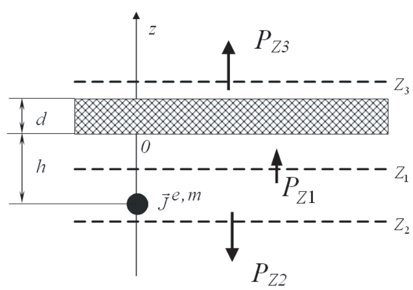

Figure 1: Parallel-plate geometry with a dielectric layer.

where $E_{x,y}$ and $H_{x,y}$ are the corresponding phasors for the tangential components of electric and magnetic field, and the asterisk stands for complex conjugating. The power through any cross-section S in the plane z is $P_z = \iint\limits_S p_z dS$.

As is done in [10], the spectral densities $U^{e,m}$ and $I^{e,m}$ of scalar electric (e) and magnetic (m) potentials are introduced, and the expansion in terms of the complete system of eigenfunctions (Fourier representation) is applied. The scalar potentials $U^{e,m}$ and $I^{e,m}$ play part of the generalized voltages and currents, respectively, and they are used instead of the unknown field components. The potentials are obtained from the rigorous solution of the boundary problem, taking into account physical effects of diffraction, absorption, refraction, and numerous reflections. The tangential components of the electromagnetic field contain spatial spectra of the scalar potentials,

$$\vec{E}_\tau = \iint\limits_{\chi_1\chi_2} (U^e\vec{t} + U^m\vec{f})d\chi_1 d\chi_2; \quad \vec{H}_\tau = \iint\limits_{\chi_1\chi_2} (I^e\vec{t} + I^m\vec{f})d\chi_1 d\chi_2. \tag{7}$$

The complete system of vector eigenfunctions is

$$\vec{t} = (-j\chi_1\vec{x}_0 - j\chi_2\vec{y}_0)e^{-j\chi_1 x - j\chi_2 y}; \quad \vec{f} = (-j\chi_2\vec{x}_0 + j\chi_1\vec{y}_0)e^{-j\chi_1 x - j\chi_2 y} \tag{8}$$

Vectors $\vec{x}_0$ and $\vec{y}_0$ are the Cartesian unit vectors. Then, the power flux is

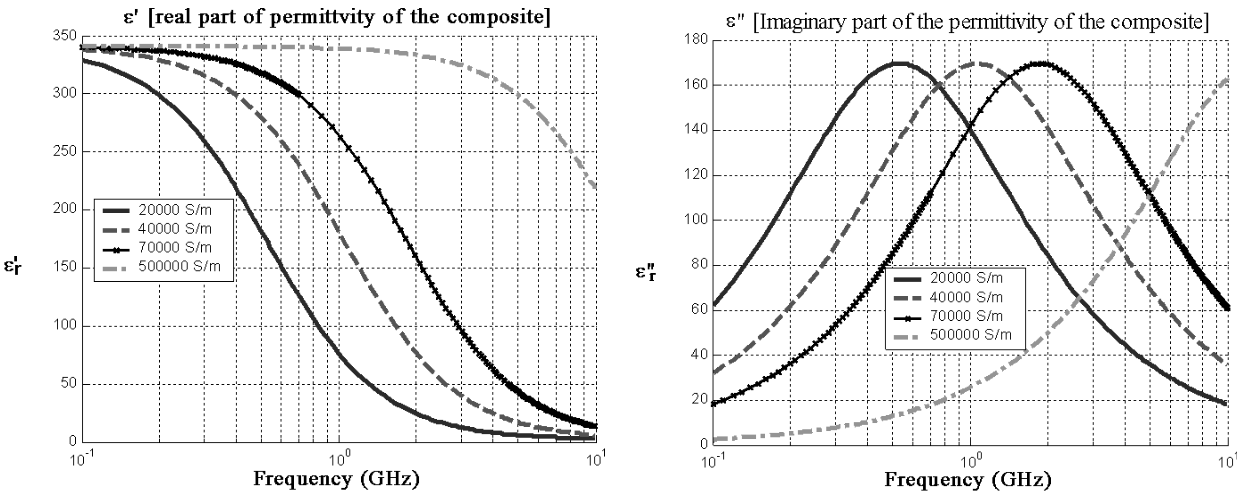

Figure 2: Complex permittivity of the composite: base material is Teflon ($\varepsilon' = 2.2$); aspect ratio for inclusions $a = 1500$; volumetric fraction of inclusions is 0.15%; conductivity of inclusions σ is a parameter.

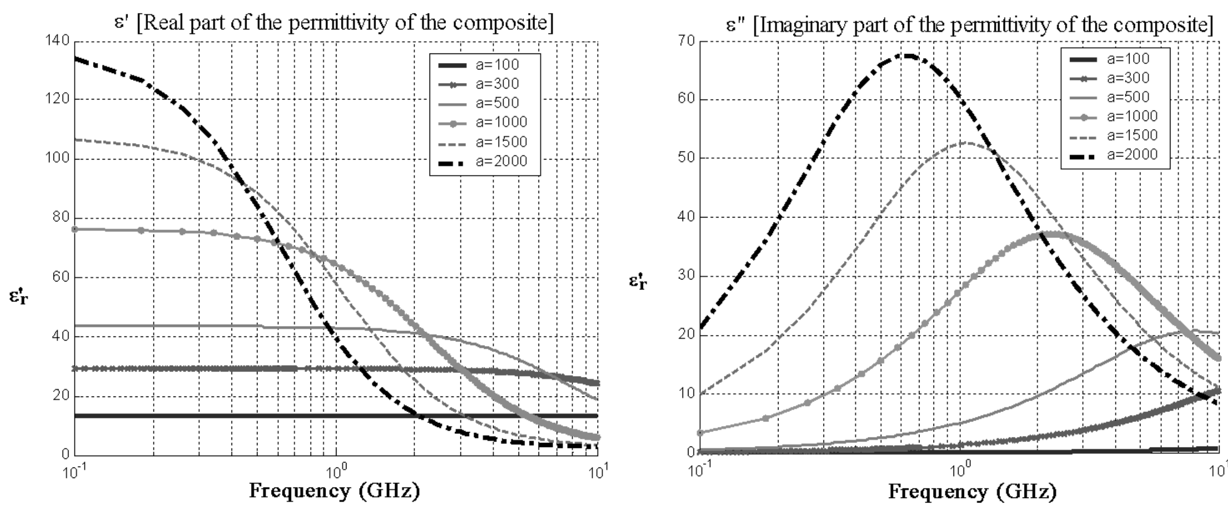

Figure 3: Complex permittivity of the composite: base material is Teflon ($\varepsilon' = 2.2$); volumetric fraction of carbon inclusions is $0.7/a < p_c$; conductivity is $\sigma = 40000\,\mathrm{S/m}^2$; aspect ratio a is a parameter.

$$P_z = 2\pi^2 Re \iint\limits_{\chi_1\chi_2} \chi^2 (U^e I^{e*} + U^m I^{m*}) d\chi_1 d\chi_2, \tag{9}$$

where $\chi^2 = \chi_1^2 + \chi_2^2$, and $\chi_{1,2}$ are the spatial frequencies along $x-$ and y-coordinates in Fourier representation for the field components. Substitution of the Fourier representation for the field components (7) into Maxwell's equations yields the 2-nd order differential equations for $U^{e,m}$ and $I^{e,m}$. In the cross-sections z_1 and z_2, where the reflected waves exist, and inside the dielectric layers, the solutions for $U^{e,m}$ and $I^{e,m}$ are

$$U^{e,m} = U^{e,m}_{inc} \cdot e^{-\gamma z} + U^{e,m}_{refl} \cdot e^{+\gamma z}, \quad I^{e,m} = (U^{e,m}_{inc} \cdot e^{-\gamma z} - U^{e,m}_{refl} \cdot e^{+\gamma z})/Z^{e,m}, \tag{10}$$

where $\gamma^2 = \chi^2 - k_0^2$ is the square of the propagation constant, and $k_0 = \omega\sqrt{\mu_0 \varepsilon_0}$ is the wave number in free space. The characteristic impedance of the medium is $Z^{e,m}$. The scalar potentials $U^{e,m}_{in}$ and $U^{e,m}_{r}$ correspond to the incident and reflected waves, respectively. They are obtained as the coefficients of two linearly independent solutions for the boundary problem formulated for the one-dimensional Helmholtz equation (in z-direction). In the cross-section z_3, there are no reflected waves, and the values $U^{e,m}_{refl}$ and $U^{e,m}_{refl}$ are zero. To calculate the power flux through the cross-section z_1 in a lossless medium, two cases should be considered: $|\chi| < k_0$, and $|\chi| > k_0$.

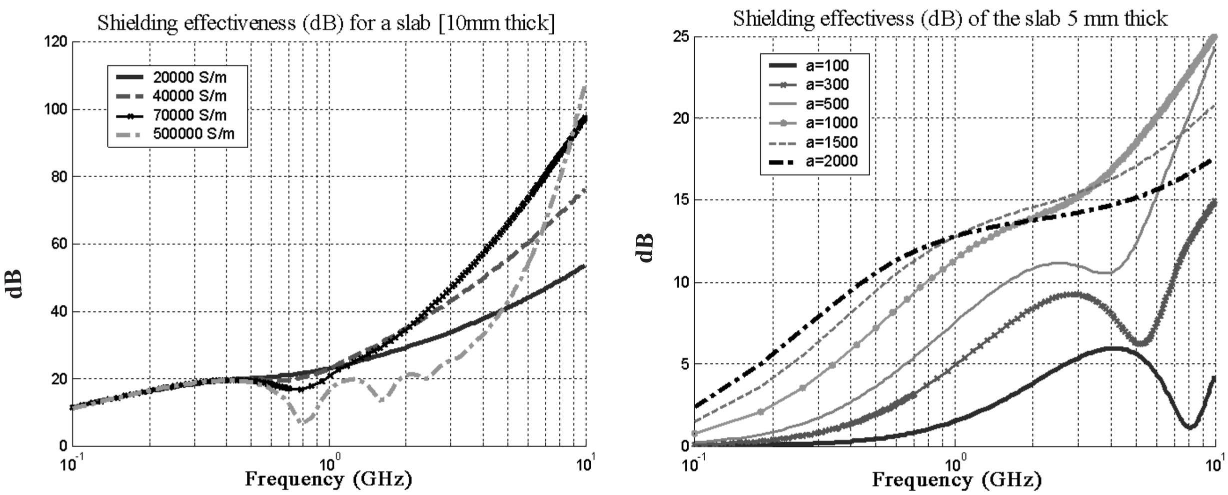

Figure 4: Shielding effectiveness (SE) in terms of plane wave formulation for an infinite layer of a composite material: (a) corresponding to Figure 2; (b) corresponding to Figure 3.

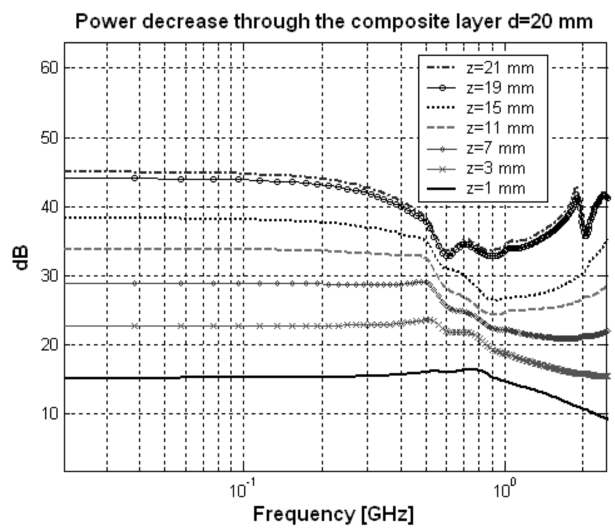

Figure 5: FDTD modeled power decrease through the composite layer. Field is radiated by the electric dipole placed at $h = 5\,\text{mm}$ below the layer (see Figure 1).

Case 1. When $|\chi| < k_0$, the propagation constant $\gamma = j\beta$ is imaginary in a lossless case, and the impedances $Z^e = \gamma/(j\omega\varepsilon_0)$ and $Z^m = j\omega\mu_0/\gamma$ are real , so the power flux for propagating waves is

$$P_{\text{z prop}} = 2\pi^2 \iint\limits_{\chi_1\chi_2} \chi^2 \Big[\Big(|U^e_{inc}|^2 - |U^e_{refl}|^2\Big)/Z^e + \Big(|U^m_{inc}|^2 - |U^m_{refl}|^2\Big)/Z^m\Big] d\chi_1\chi_2. \tag{11}$$

Case 2. When $|\chi| > k_0$, the propagation constant $\gamma = \beta$ is real, and the characteristic impedance $Z^{e,m} = jX^{e,m}$ is imaginary. The power flux for evanescent waves in this case is

$$P_{\text{z evan}} = 4\pi^2 \iint\limits_{\chi_1\chi_2} \chi^2 \Big[\text{Im}(U^e_{inc}U^{e*}_{refl})/X^e + \text{Im}(U^m_{inc}U^{m*}_{refl})/X^m\Big] d\chi_1 d\chi_2. \tag{12}$$

The exact expressions for the coefficients $U^{e,m}_{inc}$ and $U^{e,m}_{refl}$ are found from the solution of a boundary problem with the known volume densities for the source. Obviously, the power flux through the surface that crosses a medium without loss is independent of the z-coordinate, because the coefficients $U^{e,m}_{inc}$ and $U^{e,m}_{refl}$ are independent of the propagation z-coordinate. The total power flux (11), (12) is comprised of two terms: one is determined by the propagating waves ves with $\gamma = j\beta$, while the second is determined by evanescent waves with $\gamma = \beta$. Only for the regions where there are no reflected fields, ($U^{e,m}_{refl}$ and $I^{e,m}_{refl}$ are zero) the power flux is determined only by propagating waves. In general case, the propagation constant is complex. For multilayered structures, the cascading of transfer matrices can be used even for near fields, as is done in [9].

3. Computations

The frequency dependences for permittivity of the Teflon-based composites containing conductive fibers modeled using (1) are shown in Figures 2 and 3. The corresponding frequency dependences of shielding effectiveness ($SE = -20\log_{10}(E_{tr}/E_{inc})$) defined in a plane-wave formulation for infinite plane panels made of these composites are presented in Figure 4. S.E. increases with the increase of conductivity and aspect ratio of inclusions. Figure 5 shows the rate of power decrease through the absorbing layer $\eta_{trans} = -10\log_{10}(P_z/P_{ref})$. The results in Figure 5 are modeled using FDTD codes. The source is an elementary electric dipole parallel to the layer. The 20-mm thick layer is a Teflon-based ($\varepsilon_b = 2.2$) composite with conducting inclusions ($a = 100$; $\sigma = 40000\,\mathrm{S/m}$; concentration is 0.7/a, below the percolation threshold). The reference plane for calculating P_{ref} is $z = -1\,\mathrm{mm}$.

Figures 6 and 7 show the dependences of the absorption coefficient (4) versus distance of the electric dipole from the composite layer for different frequencies, conductivities of inclusions, and their aspect ratio. The electric dipole is parallel to the layer surface. When the point of observation is in the far-field region, the absorption in composites increases with the increase of conductivity and aspect ratio of inclusions. In contrast to the far-field region, in the near-field zone the higher conductivity and higher aspect ratio do not necessarily lead to greater absorption. Absorption depends on the source type, distance between the source and the layer, and the effective constitutive parameters of the composite [2]. Trends of the curves in Figures 6 and 7 at varying a and σ are different for different frequencies. This can be explained by variations in frequency dependences of the effective parameters of composites.

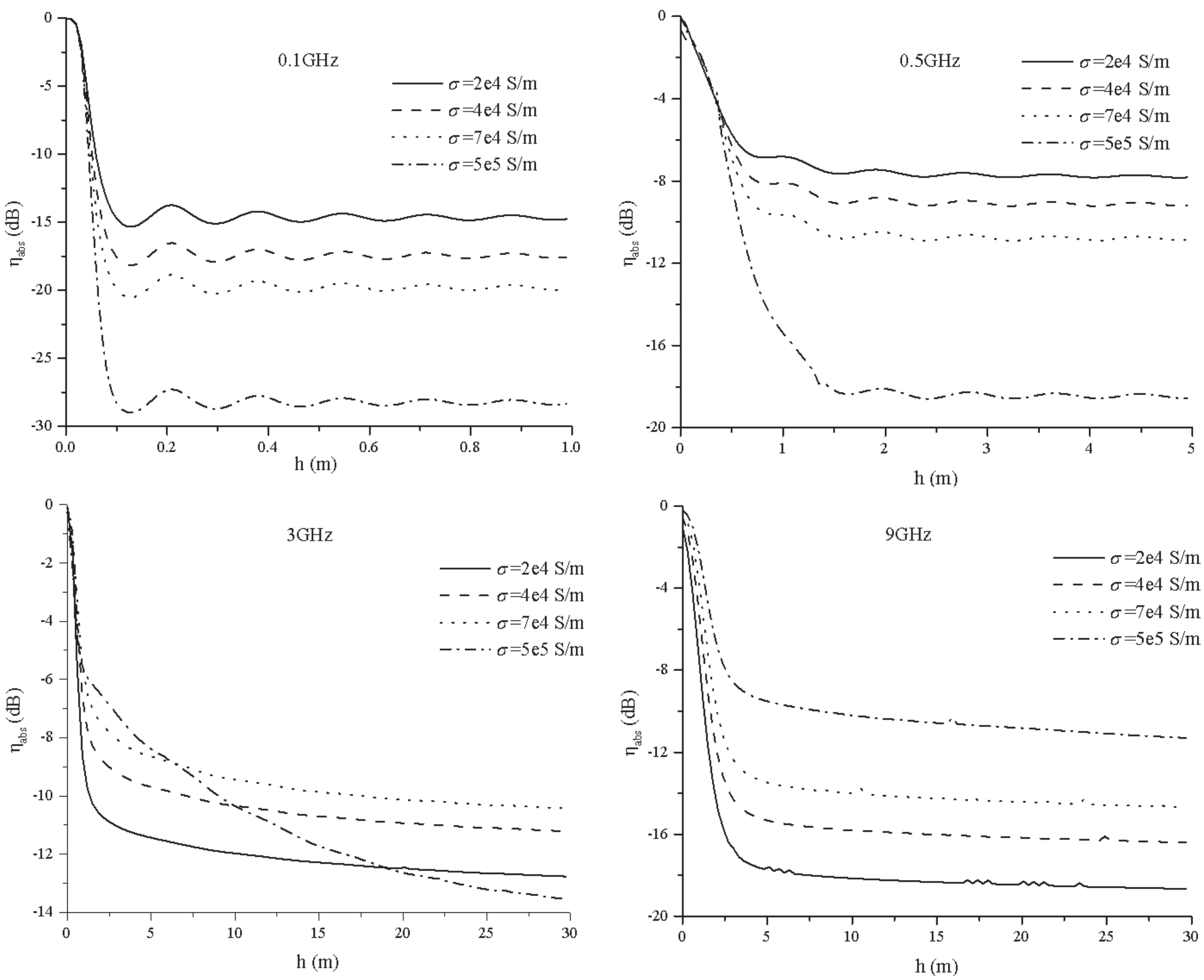

Figure 6: Absorption coefficient versus distance h between the electric dipole and the composite layer ($d = 1\,\mathrm{mm}$); frequency is 0.1 GHz, 0.5 GHz, 3 GHz, and 9 GHz. Conductivity σ of inclusions is a parameter.

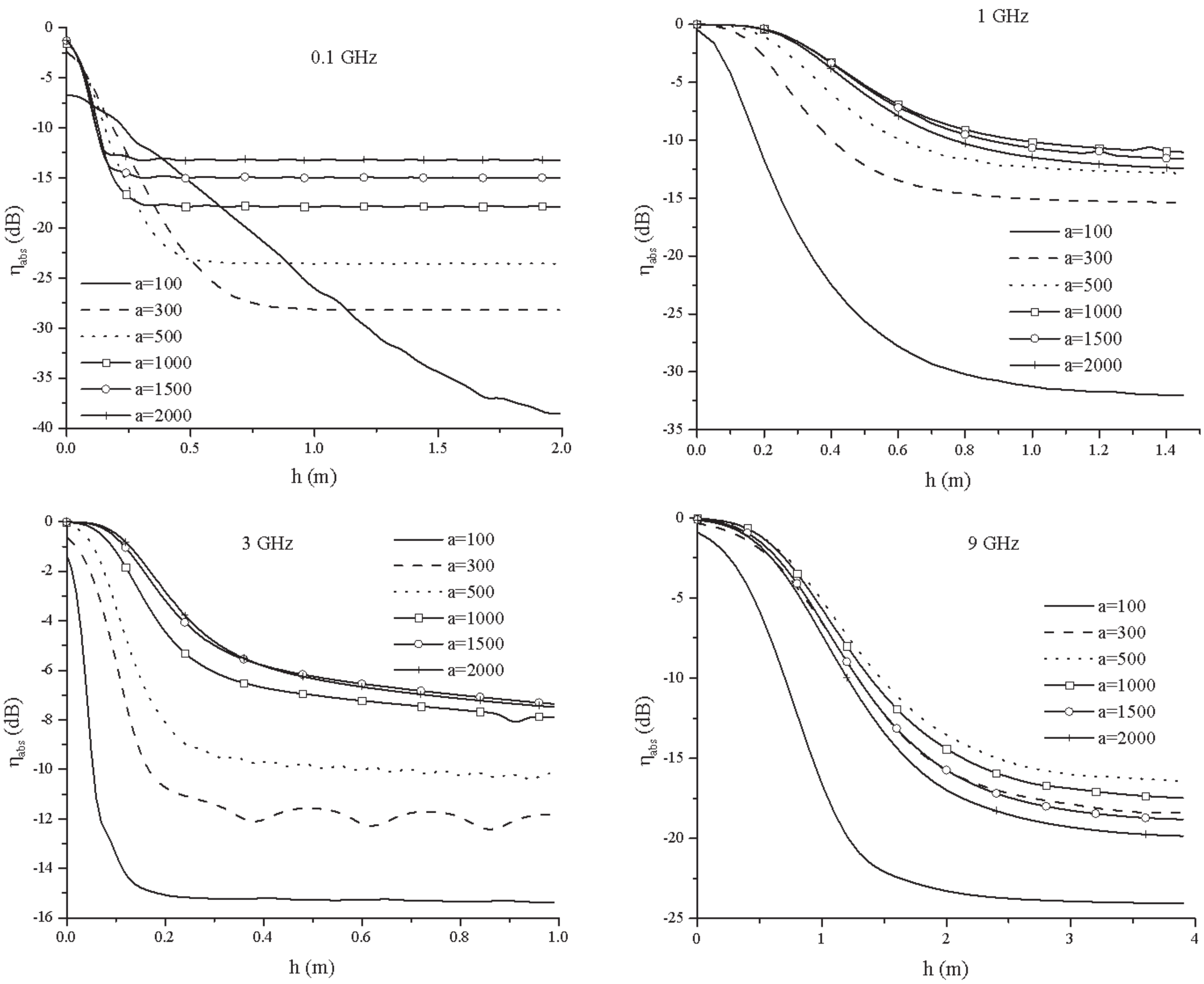

Figure 7: Absorption coefficient versus distance h between the elementary electric dipole and the composite layer (thickness $d = 1\,\mathrm{mm}$); frequency is 0.1 GHz, 1 GHz, 3 GHz, and 9 GHz. Aspect ratio a of inclusions is a parameter.

4. Conclusions

In this paper, the analytical formulas for absorption and radiation coefficients for radiators near a composite dielectric layer are obtained by rigorous boundary problem solution. The complex frequency-dependent permittivity of a composite dielectric containing conductive inclusions is modeled using Maxwell Garnett effective medium formulation. The results of computations for near-field of an elementary electric dipole close to a plane composite layer show that the behavior of absorption of near fields in the composite layer with respect to the conductivity and aspect ratio of inclusions is different from the far-field behavior. Near-field absorption in a layer depends on the distance of the radiator from the composite layer and the particular effective permittivity of the composite layer at the particular frequency.

REFERENCES

1. Koledintseva, M. Y., et al., "Engineering of composite media for shields at microwave frequencies," *Proc. IEEE EMC Symposium*, Chicago, IL, Vol. 1, 169–174, August 2005.
2. Sabirov, M., et al., "Power characteristics of radiators in multilayered dielectric structures," *Progress In Electromagnetic Research Symposium*, PIERS-04, Pisa, Italy, 409–412, March 28–31, 2004.
3. Sihvola, A., "Effective permittivity of dielectric mixtures," *IEEE Trans. Geosc. Remote Sens.*, Vol. 26, No. 4, 420–429, 1988.

4. Koledintseva, M. Y., J. Wu, J. Zhang, J. L. Drewniak, and K. N. Rozanov, "Representation of permittivity for multiphase dielectric mixtures in FDTD modeling," *Proc. IEEE Symp. Electromag. Compat.*, Santa Clara, CA, Vol. 1, 309–314, Aug. 9–13, 2004.
5. Matitsine, S. M., K. M. Hock, L. Liu, et al., "Shift of resonance frequency of long conducting fibers embedded in a composite," *J. Appl. Phys.*, Vol. 94, No. 2, 1146–1154, 2003.
6. Lagarkov, A. N. and A. K. Sarychev, "Electromagnetic properties of composites containing elongated conducting inclusions," *Physical Review B*, Vol. 53, No. 10, 6318–6336, March 1996.
7. McLachlan, D. S., A. Priou, I. Chernie, E. Isaac, and E. Henry, "Modeling the permittivity of composite materials with general effective medium equation," *Journal of Electromagn. Waves and Applications*, Vol. 6, No. 6, 1099–1131, 1992.
8. Ghosh, K. and R. Fuchs, "Spectral theory for two-component porous media," *Phys. Review B*, Vol. 38, 5222–5236, 1988.
9. Bodrov, V. V. and I. V. Sourkova, "The effect of multilayered dielectric radomes with different shapes on the amplitude and phase characteristics of antennas with planar aperture," *URSI Int. Symp. Electromagnetic Theory*, St. Petersburg, 391–393, May 1995.
10. Felsen, L. B. and N. Marcuvitz, *Radiation and scattering of waves*, Englewood Cliffs, N.J.: Prentice-Hall, Vol. 2, 1973.

The Imbedding Method in the Theory of Horn Array Antennas—Hypershort Impulses and the Near Fields

V. L. Kuznetsov
Moscow State Technical University of Civil Aviation, Russia

Abstract—The problem of hyper short impulses distortion with horn array antennas radiation considers from spectrum analysis point of view. As main reason for misphasing of Fourier-components of field the collective effect resonances of horns overirradiaton were considered. The imbedding equations for transparent coefficients (field directional diagram) and reflection coefficients of linear HAA as functions of radiated field frequency have been build. Some results of numerical experiment are given and a part of near fields (inhomogeneous modes) was discussed.

1. Introduction

The usage of nanotechnologies in radiolocation has met some problems with distortion of hyper short (HS) impulses being radiated by horn array antennas (HAA). Qualitative explanation of this effect is connected with arising of reactive fields formed near antenna's system. But quantitative description based on the traditional methods meets serious difficulties. For correct description of radiation of ultra wide band (UWB) impulse process it's necessary to examine the internal problem of electrodynamics of HAA. Let's take into consideration that models usually used to describe narrow band signals radiation can't be considered adequate for UWB impulses.

Using the spectral method distortion of UWB signal during the radiation can be explained by misphasing and changing of its Fourier-component's amplitudes, arising in horn band. The latter can be considered as a transitional layer, matching waveguides with free space. If field in feeding waveguides $-E_{in}$ and in free space $-E_{out}$ is written in the mixed representation

$$E(\vec{q}, z; \omega) = \int d\vec{\rho} \cdot E(\vec{\rho}, z; \omega) \exp\{-i\vec{q}\vec{\rho}\}, \qquad \vec{\rho} = (x, y), \tag{1}$$

than the main characteristic of HAA—the transparence coefficient $T(\vec{q}, \vec{q}'; \omega)$ can be determent as a kernel of integral equation

$$E_{out}(\vec{q}, z; \omega)\big|_{z=H} = \int d\vec{q}'\, T(\vec{q}, \vec{q}'; \omega) \cdot E_{in}(\vec{q}', z; \omega)\Big|_{z=0} \tag{2}$$

Here H is thickness of the transition layer or horns height.

It's clear that when describing UWB impulse radiation in terms of spectral theory the demand to the measurement accuracy $T(\vec{q}, \vec{q}'; \omega)$ is much bigger than in the case of narrow band signal. In particular, the wide spectrum of the signal forces to take into consideration the group effects—i. e., overirradiation of horns in grating. This is usually neglected in narrowband field. Periodic property of grating space structure in combination with wide space signal spectrum leads to the fact that the definite group of frequencies inevitably lays in the field of Wood anomalies, where the important role is played by near fields—inhomogeneous modes of space spectrum of the radiation field.

Thus, the basic problem at the spectral approach to the solution of a problem on radiation of UWB-impulses by HAA consists in a choose of method allowing to solve the internal problem of HAA electrodynamics maximum correctly and to describe amplitude, phase and spatial vector of radiation of a monochromatic signal as function of its frequency. As such an approach it is proposed to use the imbedding method.

2. Imbedding Equations for Linear HAA

The imbedding method is used as base for getting the equation for transparent coefficient of HAA. The kernel of this method is in the following. A great number of solutions of similar problems is examined, these problems differ only with the value of one parameter—the imbedding parameter. In the considered case such a parameter is the height of the horn h—transparent layer thickness. The "utmost" solutions are: the field radiated by the system of the feeding waveguides ($h = 0$) and the field of researched HAA ($h = H$). Farther the solutions evolution equation is built in this functional space. Thus there can be established the connection between the solutions of the problems with corresponding different values of the parameter. The solution with one value of the imbedding parameter is relatively simple and is taken as known ($h = 0$). Than the solution of the researched problem ($h = H$) can be received as the solution of the Cauchy problem for imbedding equation (first order differential equation) with the initial condition as a solution of the problem at $h = 0$. Let's take into consideration that problems of waveguides radiation ($h = 0$) are rather simpler than problem of HAA radiation ($h = H$).

Thus, the transition from electrodynamics characteristics of waveguides' cut ($h = 0$) to the corresponding characteristics of horns can be seen in describing intermediate systems—the elements of the truncated horns family received one from another by increasing the height of the walls as it's shown in Fig. 1

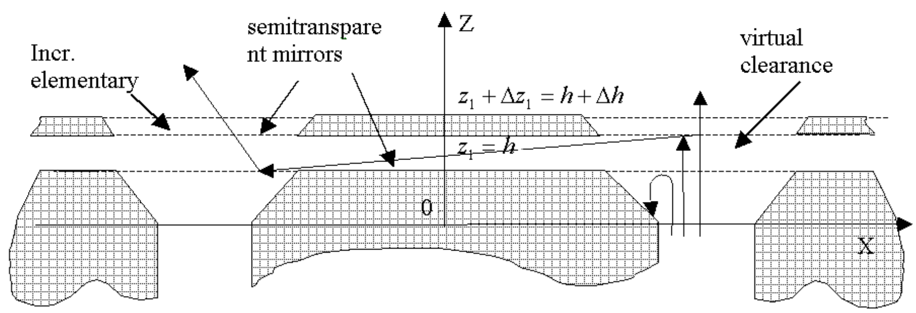

Figure 1: The evolution of horn layer under increasing the imbedding parameter.

To make the problem simpler let's use the method of periodical prolongation of the structure, i. e., let's add the researched HAA, consisting of N horns, with identical systems to the left and to the right to make it periodical structure. Under such a representation of horn grating its space spectrum of radiation becomes discrete. From the mathematical point of view it means that we change integral equations to matrix equations.

Farther it is necessary to express the transparence coefficient of "increased" HAA $T(h + \Delta h)$ in terms of $T(h)$, the reflection coefficient $r(h, \Delta h)$ and transparence coefficient $t(h, \Delta h)$ of the elementary layer.

According to the ideology of the works [1–2] the field being necessary for calculating $T(h+\Delta h)$ is considered in endless thin (virtual) clearance that divides the truncated horn of height h from the increased elementary layer. The clearance borders can be considered semitransparent mirrors with transparent coefficients $r(h, \Delta h)$ and $R(h)$. Here $R(h)$ it is a reflection coefficient and of truncated HAA of height h. Taking into consideration multiple reflections of field from the layer's borders the next equation [3] takes place

$$T(h + \Delta h) = [R(h + \Delta h) - r(h + \Delta h, \Delta h)] \cdot t^{-1}(h + \Delta h, \Delta h) \cdot R^{-1}(h) \cdot T(h), \tag{3}$$

written in finite difference.

Imbedding equation (3) is not closed, there is an unknown function $R(h)$ in it. The equation for reflection coefficient for truncated HAA can be received by variation of co-relations of integral equations method also known as MMM [4]. This method gave good results in the description of reflection from ideally conducting surfaces.

The distinctive part of the problem for HAA is the presence of waveguides—special insertions in ideally conducting surfaces. On these parts of the surface the Dirichlet condition doesn't take place that leads to essential complication of the method equation. Generalizing of method equations can be received knowing that the field in the spaces where Dirichlet condition doesn't take place can be represented as the superposition of waveguide's modes.

The equation for $R(h)$, evident view of which has being shown in [5] is a following matrix Riccati equation

$$\frac{1}{2i}\frac{d\hat{R}}{dz} = \hat{R}(\hat{I} - \hat{\widetilde{D}})\hat{V}^{-1} - \hat{R}\left[\hat{\widetilde{D}}(\hat{I} - \hat{H}\hat{V}) + (\hat{I} - \hat{\widetilde{D}})\hat{H}\hat{V}\right]\hat{V}^{-1}\hat{R} + (\hat{I} - \hat{H}\hat{V})\hat{V}^{-1}\hat{R} \tag{4}$$

Here $\hat{\widetilde{D}} = \hat{W}^{-`1}\hat{\widetilde{C}}^{-1}\hat{F}$, $\hat{H} = \hat{F}\hat{K}^{-1}\hat{W}^{-1}$, $\hat{K} = \hat{V}\hat{C} - \frac{1}{\Lambda}\hat{\mu}$. Matrix $\hat{\widetilde{C}}$ has the following components $\widetilde{C}_{kl} = \frac{1}{\Lambda}\int\limits_0^{\Lambda} e^{-i\frac{2\pi}{\Lambda}(k-l)x+iv_l h(x)}dx$, and matrix $\widetilde{C} - C_{kl} = \frac{1}{\Lambda}\int\limits_0^{\Lambda} e^{-i\frac{2\pi}{\Lambda}(k-l)x-iv_l h(x)}dx$, $h(x)$ is the form of a horn's profile, $A_{kn} = \int\limits_0^{\Lambda} dx \int\limits_{-\infty}^{\infty} dx' H_0^{(1)}(x, x', h(x), h(x')) \cdot e^{-iq_k x+iq_n x'}$, $\mu_{kn} = \frac{4}{b} \cdot \sum\limits_{p=1}^{\infty} \widetilde{\chi}_{kp}\frac{1}{\widetilde{\nu}_p}\chi_{kp}$, $\widetilde{\nu}_p = \sqrt{k_0^2 - \widetilde{q}_p^2}$, $\widetilde{q}_p = \frac{\pi}{b}p$, b is waveguide width, $\chi_{pn} = \int\limits_{\frac{\Lambda-b}{2}}^{\frac{\Lambda+b}{2}} \varphi_p(x - \frac{\Lambda - b}{2}) \cdot e^{iq_n x} dx$, $\varphi_p(\cdot)$ is p-th waveguide's mode, $\hat{\tilde{\chi}} = \hat{\chi}^{*T}$, $W_{mn} = e^{iv_n z_1} \cdot \delta_{nm}$, δ_{nm} is Kronecker's symbol, $\hat{I}$ is identity matrix. $F_{kn} = \frac{2}{\Lambda} x \cdot \sin c\left[\frac{2}{\Lambda}(k-n)x\right]$, matrix $\hat{V}$ is diagonal with elements $v_{pk} = \frac{2}{v_k} \cdot \delta_{kp}$.

As the initial condition for it serves the reflection coefficient of system of feeding waveguides, which could be found by using the mode-matching method.

3. A Physical Picture of Distortions of a UWB Signal at Radiation by HAA. Wood Resonance and Near Fields

Periodic expansion of HAA used in the stated approach allows not only to simplify a problem in mathematical aspect, but also to make more clear interpretation of destruction mechanism of the signal's form. It is known, that at interaction of a field with periodic structure there only components of a discrete spectrum are interconnected. In case of linear HAA it is possible to present a set of the wave vectors forming this spectrum, as $\vec{k}_n = (\nu_n, q_0 + nk)$, here $k = 2\pi/\Lambda$—is a vector of the inverse lattice, Λ is distance between the nearest radiators, $n \in Z$, $\nu_n = \sqrt{k^2 - (q_0 + nk)^2}$ and q_0 is a corresponding projection of allocated components of field angular spectrum. In case of the scattering problem, usually it is a projection of an external field's wave vector.

If frequency of a field $\omega = ck$ is such that one of its space components gets in area of Wood resonance $\nu_n \cong 0$, then anomalies are observed in distribution of a field on modes.

At radiation of the narrowband signal, carrying (central) frequency is chosen so that the condition $\lambda_0 > \Lambda\,(k_0 < \frac{2\pi}{\Lambda})$ is satisfied. In this case in a space spectrum of radiation only one mode is homogeneous (lateral petals in the directional diagram are absent). Thus all field modes, both homogeneous, and inhomogeneous, are far from Wood's resonance (Fig. 2 (a)). Therefore the problem of distortion of the form of the narrowband signal usually does not arise.

For a UWB signal the range of wave numbers change is great. It grasps a lot of resonant points (Fig. 2 (b)).

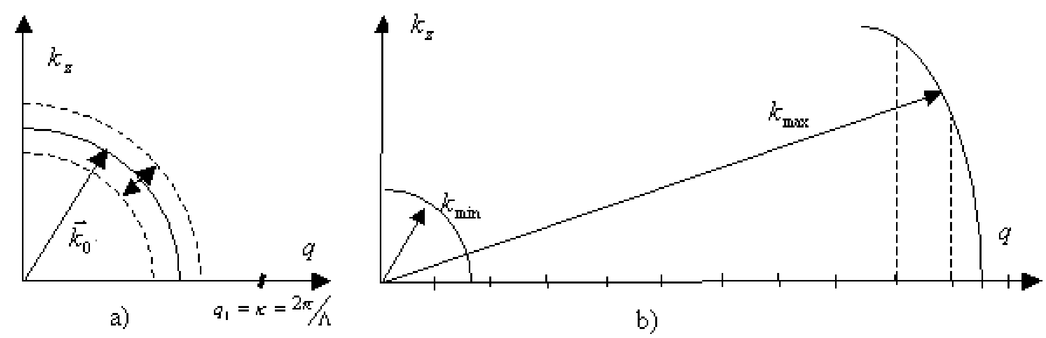

Figure 2: The range of wave numbers change for narrowband -(a) and UWB -(b) signal.

As follows from the formula (1), the transparency coefficient (the directional diagram) HAA is substantially determined by the feature of matrix reflection coefficient $R(h)$. Let's present its elements as

$$R_{n,m}(\omega) = |R_{n,m}(\omega)| \cdot \exp\{i\Phi_{n,m}(\omega)\}$$

The magnitude $\tau_{n,m}(\omega) = -\frac{d}{d\omega}\Phi_{n,m}(\omega)$ defines a group delay for n-th mode of a scattering field. The index m defines an external field wave vector $\nu_m = \sqrt{k^2 - (q_0 + k \cdot m)^2}$. If $\tau_{n,m}(\omega)$ varies with change of frequency then the output form of a signal most likely is distort. In other words, any deviation of frequency dependence $\tau_{n,m}(\omega)$ from the linear law must be analyzed.

On Fig. 3 diagrams of dependences $|R_{n,m}(k')|$ and $\Phi(k')$ are presented. They are calculated with the help of imbedding method represented for a case of normal falling ($q_0 + k \cdot m = 0$) of an external field on the periodic surface modeling linear HAA.

Here wave parameter k' is a dimensionless wave vector $k' = k\Lambda/2\pi = \omega'$. Let's notice, that deviations from linear dependence near the values of parameter $k' = n$, $n \in Z$ corresponding to points of Wood's resonance, are observed.

Let's note also, that far from resonant points, the kind of dependence $\Phi = \Phi(\omega')$ can be counted linear, but in the different areas of a frequency spectrum separated by resonant values of parameter, the corner of

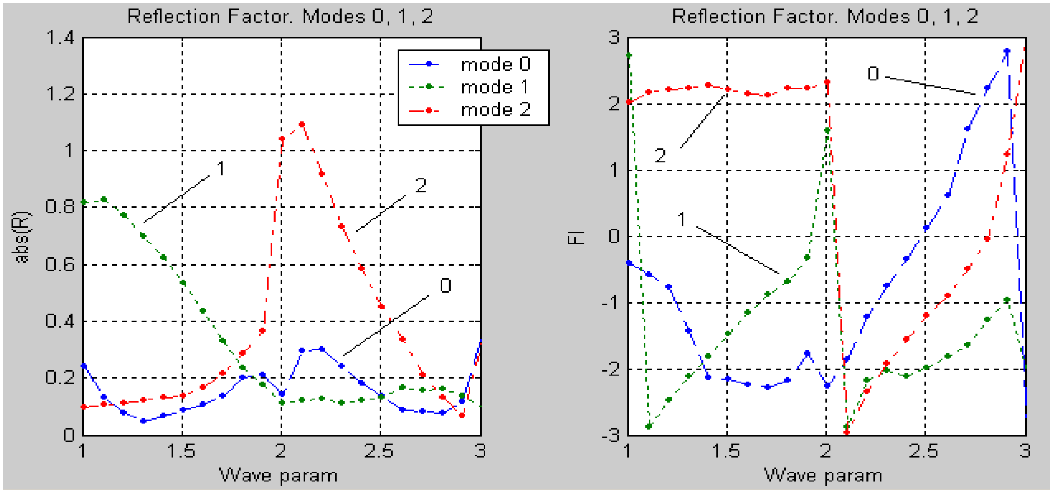

Figure 3: The diagrams of dependences $|R_{n,m}(k')|$ and $\Phi(k')$.

an inclination of curves essentially differs. As the spectrum of a UWB signal spans the big number of such areas even without taking into account Wood's anomalies dependence $\Theta = \Theta(\omega')$ can be approximated only by wiselinear, but not linear dependence. It also is necessary to take into account at the analysis of the reasons of the distortion of the form of radiated signal.

Complete results of the carried out numerical experiment will be submitted in the report.

4. Conclusion

The problem of ultra short impulses radiated by HAA is observed. From the spectrum analysis point of view impulse distortion depends on its Fourier components misphasing. To describe this effect the matrix transparence coefficient $\hat{T}(\omega)$ of horns layer is introduced as transitional layer that matches waveguides with free space. To calculate $\hat{T}(\omega)$ the imbedding equations were built. They allow considering horns overirradiation effects and borders effects that bound with its finite dimensions. Group delay variation that leads to signal disintegration can be represented as resonant interactions (Wood anomalies).

Reactive fields formed near antenna's system can be represented as superposition of inhomogeneous modes. The importance of near fields (inhomogeneous modes) grows sharply near the points of Wood resonant.

This quality summary were confirmed by diagrams of $R_{nm}(\omega)$ dependence that were calculated using imbedding equations describing external field interactions with periodical surface that models linear HAA.

REFERENCES

1. Barabanenkov, Y. N., V. L. Kuznetsov, and M. Y. Barabanenkov, "Progress in electromagnetic research," *PIER*, Vol. 24, 39–75, 1999.
2. Barabanenkov, Y. N. and V. L. Kuznetsov, *Radiotechnika I Elektronika*, Vol. 44, No. 6, 659, 1999 (in Russian).
3. Bakhrakh, L. D., V. L. Kuznetsov, and I. I. Vizgina, Antennas, No. 8–9, 42, 2004 (in Russian).
4. Masel, R. I., R. P. Merril, and W. H. Miller, Http:// Phys. Rev. B., Vol. 12, No. 12, 5545, 1975.
5. Bakhrakh, L. D., V. L. Kuznetsov, and I. I. Vizgina, *Nauchnii Westnik Mstuca, Series Mathematic and Physic*, No. 91, 48–62, 2005.

Near-field Response in Lossy Media with Exponential Conductivity Inhomogeneity

R. J. Riddolls
Defence R&D Canada–Ottawa, Canada

Abstract—This paper examines the near-field response to source currents in lossy media with exponential conductivity inhomogeneity. The motivation for this work is to understand the modification of the polar ionosphere D region (50–90 km altitude) by powerful high frequency transmitters. The transmitted waves heat the D region plasma, causing a localized conductivity perturbation. In the presence of the DC electric field of the polar electrojet, the conductivity perturbation produces a current perturbation referred to as "antenna current" that can drive extremely/very low frequency radiation. Here we seek to understand the production of antenna current in a strongly inhomogeneous plasma. In the lower D region, the static approximation is valid, and we solve using a scalar potential description. In the upper D region, we use the magnetoquasistatic approximation and solve using a vector potential approach.

1. Introduction

We begin the formulation by defining standard scalar and vector potentials for the electric and magnetic field perturbations introduced by the conductivity perturbation. In time-harmonic form, we have

$$\mathbf{E} = i\omega\mathbf{A} - \nabla\Phi \qquad\qquad \mathbf{B} = \nabla\times\mathbf{A}, \tag{1}$$

where i is the imaginary unit and ω is frequency. Let us suppose that the charge relaxation time and electromagnetic transit time are both small compared to the time scale of interest. This assumption allows us to ignore the effect of displacement current, so that current consists of only the imposed antenna current $\mathbf{J}_s$ due to the conductivity perturbation, and a self-consistent conduction current $\sigma\mathbf{E}$, where σ is the conductivity of the medium. Adopting a Coulomb gauge, the wave equation is given by

$$\nabla^2\mathbf{A} + i\omega\mu_0\sigma\mathbf{A} = -\mu_0\mathbf{J_s} + \mu_0\sigma\nabla\Phi, \tag{2}$$

where μ_0 is the permeability of the medium, assumed the same as free space. The two terms on the right side can be viewed as source terms for the vector potential. We will proceed as follows. In the lower ionosphere D region, the conductivity is small such that the magnetic relaxation time is fast compared to the time scale of interest, and thus we ignore effects of vector potential. In the upper D region, the conductivity is large such that the magnetic relaxation time is slower than the time scale of interest. In this case, magnetic diffusion dominates the behaviour of the system, and we ignore the effects of space charge and its associated scalar potential. We will analyze each of the two limits.

The above statements assume a simple scalar conductivity. In practice, the plasma conductivity is anisotropic and requires a matrix representation. In the northern polar region the direction z (altitude) is antiparallel the earth's magnetic field. The appropriate conductivity tensor is given by

$$\boldsymbol{\sigma} = e^{hz}\begin{bmatrix} \sigma_P & \sigma_H & 0 \\ -\sigma_H & \sigma_P & 0 \\ 0 & 0 & \sigma_0 \end{bmatrix}, \tag{3}$$

where $1/h$ is the scale height of the conductivity. Here, the exponential factor models the variability in the plasma conductivity due to the plasma density inhomogeneity, and the matrix entries are constants pertaining to the anisotropic plasma conductivity tensor. The quantity σ_P is the Pedersen conductivity, σ_H is the Hall conductivity, and σ_0 is the specific conductivity. We are assuming that all conductivities vary in altitude at the same rate. Strictly speaking this is not the case as the specific conductivity increases with altitude somewhat more rapidly than the Pedersen or Hall conductivities. However, for the purposes of a simple treatment, we ignore the fine details of the altitude dependence of the individual conductivity elements.

2. Static Solution

We now turn to the problem of determining the scalar potential Φ in the static limit. If we incorporate the tensor definition for $\boldsymbol{\sigma}$ into Equation (2), ignore the vector potential, and take the divergence of both sides, we find that

$$\nabla^2\Phi + \left(\frac{\sigma_0}{\sigma_P} - 1\right)\frac{\partial^2\Phi}{\partial z^2} + \frac{h\sigma_0}{\sigma_P}\frac{\partial\Phi}{\partial z} = \frac{e^{-hz}}{\sigma_P}\nabla\cdot\mathbf{J}_s \equiv S(\mathbf{r}), \tag{4}$$

where $S(\mathbf{r})$ is the source distribution. Let us expand the right and left sides of Equation (4):

$$S(\mathbf{r}) = \int_{-\infty}^{\infty}\int_{-\infty}^{\infty}\int_{-\infty}^{\infty} d\mathbf{r}_0 S(\mathbf{r}_0)\delta(\mathbf{r}-\mathbf{r}_0) \tag{5}$$

$$\Phi(\mathbf{r}) = \int_{-\infty}^{\infty}\int_{-\infty}^{\infty}\int_{-\infty}^{\infty} d\mathbf{r}_0 S(\mathbf{r}_0)G_\Phi(\mathbf{r},\mathbf{r}_0). \tag{6}$$

Inserting these expansions into Equation (4) yields an expression for the Green's function $G_\Phi(\mathbf{r},\mathbf{r}_0)$:

$$\nabla^2 G_\Phi(\mathbf{r},\mathbf{r}_0) + \left(\frac{\sigma_0}{\sigma_P} - 1\right)\frac{\partial^2 G_\Phi(\mathbf{r},\mathbf{r}_0)}{\partial z^2} + \frac{h\sigma_0}{\sigma_P}\frac{\partial G_\Phi(\mathbf{r},\mathbf{r}_0)}{\partial z} = \delta(\mathbf{r}-\mathbf{r}_0). \tag{7}$$

This is a constant coefficient equation, and therefore $G_\Phi(\mathbf{r},\mathbf{r}_0)$ is the same as $G_\Phi(\mathbf{r}-\mathbf{r}_0)$. We can write

$$\nabla^2 G_\Phi(\mathbf{r}) + \left(\frac{\sigma_0}{\sigma_P} - 1\right)\frac{\partial^2 G_\Phi(\mathbf{r})}{\partial z^2} + \frac{h\sigma_0}{\sigma_P}\frac{\partial G_\Phi(\mathbf{r})}{\partial z} = \delta(\mathbf{r}). \tag{8}$$

This equation solves easily using the method of Fourier transforms. Taking the Fourier transform of Equation (8), solving for $G_\Phi(\mathbf{k})$, and then inverse transforming, results in the following solution for $G_\Phi(\mathbf{r})$:

$$G_\Phi(\mathbf{r}) = -\frac{1}{8\pi^3}\int_{-\infty}^{\infty}\int_{-\infty}^{\infty}\int_{-\infty}^{\infty} d\mathbf{k}\frac{e^{i\mathbf{k}\cdot\mathbf{r}}}{k_x^2 + k_y^2 + (\sigma_0/\sigma_P)k_z^2 - ih(\sigma_0/\sigma_P)k_z}. \tag{9}$$

We can now convert Equation (9) to cylindrical co-ordinates (ρ,ϕ,z) and (k_ρ,α,k_z) and perform the integrals:

$$\begin{aligned}
G_\Phi(\mathbf{r}) &= -\frac{1}{8\pi^3}\int_0^\infty dk_\rho k_\rho \int_{-\infty}^{\infty} dk_z \frac{e^{ik_z z}}{k_\rho^2 + (\sigma_0/\sigma_P)k_z^2 - ih(\sigma_0/\sigma_P)k_z}\int_0^{2\pi} d\alpha e^{ik_\rho\rho\cos(\phi-\alpha)} &(10)\\
&= -\frac{1}{4\pi^2}\int_0^\infty dk_\rho k_\rho J_0(k_\rho\rho)\int_{-\infty}^{\infty} dk_z \frac{e^{ik_z z}}{k_\rho^2 + (\sigma_0/\sigma_P)k_z^2 - ih(\sigma_0/\sigma_P)k_z} &(11)\\
&= -\frac{e^{-hz/2}}{2\pi\sigma_0/\sigma_P}\int_0^\infty dk_\rho \frac{k_\rho J_0(k_\rho\rho)e^{-\sqrt{(h/2)^2+(\sigma_P/\sigma_0)k_\rho^2}|z|}}{\sqrt{(h/2)^2 + (\sigma_P/\sigma_0)k_\rho^2}} &(12)\\
&= -\frac{e^{-hz/2 - h\sqrt{(\sigma_0/\sigma_P)\rho^2+z^2}/2}}{4\pi\sqrt{(\sigma_0/\sigma_P)\rho^2 + z^2}}. &(13)
\end{aligned}$$

The integral over k_z above is facilitated by the residue theorem, and the integral over k_ρ uses the following identity

$$\int_1^\infty du e^{-\alpha u}J_0(\beta\sqrt{u^2-1}) = \frac{e^{-\sqrt{\alpha^2+\beta^2}}}{\sqrt{\alpha^2+\beta^2}}, \tag{14}$$

which can be found in standard tables. The scalar potential for a given source distribution can then be found by integrating this Green's function over the source distribution. The basic form of the scalar potential is similar to that of sources in homogeneous isotropic media, except there is exponential decay in the upward direction, and the potential is squeezed in the ρ direction compared to the z direction by a factor corresponding to the degree of anisotropy σ_0/σ_P. We also note that the Hall conductivity σ_H does not play a factor in the static scalar potential.

3. Static Solution Example

In this section, we provide an example of the static solution. Let us consider a current source $\mathbf{J}_s$ that consists of a horizontal cylinder-like structure modelled by

$$\mathbf{J}_s = \hat{\mathbf{x}}I\delta(y)\delta(z)[\mu(x+L/2) - \mu(x-L/2)], \tag{15}$$

where I is the current and L is the cylinder length. The source distribution is given by

$$\begin{aligned} S(\mathbf{r}_0) &= (e^{-hz}/\sigma_P)\nabla\cdot\mathbf{J}_s & (16)\\ &= (I/\sigma_P)[\delta(\mathbf{r}_0+\hat{\mathbf{x}}L/2)-\delta(\mathbf{r}_0-\hat{\mathbf{x}}L/2)]. & (17)\end{aligned}$$

The potential is given by

$$\begin{aligned}\Phi(\mathbf{r}) &= \int_{-\infty}^{\infty}\int_{-\infty}^{\infty}\int_{-\infty}^{\infty} d\mathbf{r}_0 S(\mathbf{r}_0)G_\Phi(\mathbf{r}-\mathbf{r}_0) & (18)\\ &= \frac{Ie^{-hz/2}}{4\pi\sigma_P}\left\{\frac{e^{-h\sqrt{(\sigma_0/\sigma_P)[(x-L/2)^2+y^2]+z^2}/2}}{\sqrt{(\sigma_0/\sigma_P)[(x-L/2)^2+y^2]+z^2}}-\frac{e^{-h\sqrt{(\sigma_0/\sigma_P)[(x+L/2)^2+y^2]+z^2}/2}}{\sqrt{(\sigma_0/\sigma_P)[(x+L/2)^2+y^2]+z^2}}\right\}. & (19)\end{aligned}$$

The total current $\mathbf{J}=\mathbf{J}_s-\boldsymbol{\sigma}\cdot\nabla\Phi$, near the z axis, is given by:

$$\begin{aligned}\mathbf{J}_{(x,y)\approx 0} &= (\mathbf{J}_s-\boldsymbol{\sigma}\cdot\nabla\Phi)_{(x,y)\approx 0} & (20)\\ &= \hat{\mathbf{x}}I\delta(y)\delta(z)-(\hat{\mathbf{x}}\sigma_P-\hat{\mathbf{y}}\sigma_H)IL\sigma_0(1+hw/2)\exp[h(z-w)/2]/(4\pi\sigma_P^2 w^3), & (21)\end{aligned}$$

where $w=\sqrt{(\sigma_0/\sigma_P)(L/2)^2+z^2}$. The conduction current $-\boldsymbol{\sigma}\cdot\nabla\Phi$ flows largely above the origin, opposite the source current, effectively forming a vertical current loop. The conduction current distributions are shown for $L = 15$ km and the cases of homogeneous isotropic, inhomogeneous isotropic, and inhomogeneous anisotropic media.

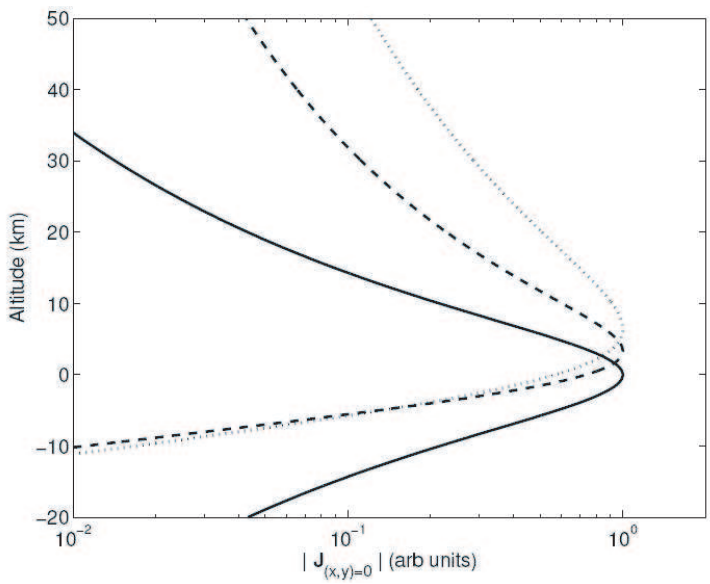

Figure 1: Static conduction current distributions. Solid line: homogeneous isotropic media. Dashed line: inhomogeneous isotropic media ($1/h = 2.5$ km). Dotted line: inhomogeneous anisotropic media ($1/h = 2.5$ km, $\sigma_0/\sigma_P = 2$).

4. Magnetoquasistatic Solution

Let us now consider the problem of determining the vector potential relevant to the magnetoquasistatic limit. Returning to Equation (2), we ignore the scalar potential so that we have

$$\nabla^2\mathbf{A}+i\omega\mu_0\boldsymbol{\sigma}\cdot\mathbf{A}=-\mu_0\mathbf{J}_s. \qquad (22)$$

By Equation (4), the z component is decoupled from the x and y components. Since the current perturbation $\mathbf{J}_s$ is generally horizontally directed in practical situations, A_z is not driven, and we assume it is zero. The x and y components are decoupled by transforming to a basis of eigenvectors of the conductivity tensor:

$$\begin{bmatrix}\hat{A}_x\\ \hat{A}_y\end{bmatrix}=\frac{1}{\sqrt{2}}\begin{bmatrix}1 & -i\\ 1 & i\end{bmatrix}\begin{bmatrix}A_x\\ A_y\end{bmatrix}. \qquad (23)$$

After the transformation the equations for the vector potential components $\hat{A}_x$ and $\hat{A}_y$ can be written as

$$\nabla^2 \begin{bmatrix} \hat{A}_x \\ \hat{A}_y \end{bmatrix} + i\omega\mu_0 e^{hz} \begin{bmatrix} \sigma_P + i\sigma_H & 0 \\ 0 & \sigma_P - i\sigma_H \end{bmatrix} \begin{bmatrix} \hat{A}_x \\ \hat{A}_y \end{bmatrix} = -\frac{\mu_0}{\sqrt{2}} \begin{bmatrix} J_{sx} - iJ_{sy} \\ J_{sx} + iJ_{sy} \end{bmatrix} \equiv -\mu_0 \hat{\mathbf{J}}_s. \tag{24}$$

The Green's function for a component of $\hat{\mathbf{A}}$ is given by

$$\Big[\nabla^2 + i\omega\mu_0 e^{hz}(\sigma_P \pm i\sigma_H)\Big] G_{\hat{A}}(\mathbf{r}, \mathbf{r}_0) = \delta(\mathbf{r} - \mathbf{r}_0). \tag{25}$$

In view of the e^{hz} factor, $G_{\hat{A}}(\mathbf{r}, \mathbf{r}_0) = G_{\hat{A}}(x - x_0, y - y_0, z, z_0) \neq G_{\hat{A}}(\mathbf{r} - \mathbf{r}_0)$. Thus we write

$$\Big[\nabla^2 + i\omega\mu_0 e^{h(z+z_0)}(\sigma_P \pm i\sigma_H)\Big] G_{\hat{A}}(x, y, z + z_0, z_0) = \delta(\mathbf{r}). \tag{26}$$

A solution by the method of Fourier transforms is confounded by the e^{hz} factor. Thus we transform in the x and y directions only, which converts the partial differential Equation (25) into an ordinary differential equation:

$$\Big[\frac{\partial^2}{\partial z^2} - k_\rho^2 + i\omega\mu_0 e^{h(z+z_0)}(\sigma_P \pm i\sigma_H)\Big] G_{\hat{A}}(k_x, k_y, z + z_0, z_0) = \delta(z). \tag{27}$$

The solutions are the Bessel functions $J_\nu[\lambda e^{h(z+z_0)/2}]$ and $Y_\nu[\lambda e^{h(z+z_0)/2}]$, with $\lambda = 2\sqrt{i\omega\mu_0(\sigma_P \pm i\sigma_H)}/h$ and $\nu = 2k_\rho/h$. In the $z \to \infty$ limit, the only bounded linear combination of solutions for $0 < \arg(\lambda) < \pi$ is a Hankel function of the form $C_1 H_\nu^{(1)}[\lambda e^{h(z+z_0)/2}]$. Similarly, in the $z \to -\infty$ limit, the only bounded solution for all complex λ is a Bessel function of the form $C_2 J_\nu[\lambda e^{h(z+z_0)/2}]$. To determine the constants C_1 and C_2 we impose that the solutions in the regions $z > 0$ and $z < 0$ are continuous at $z = 0$:

$$C_1 H_\nu^{(1)}\big(\lambda e^{hz_0/2}\big) - C_2 J_\nu\big(\lambda e^{hz_0/2}\big) = 0, \tag{28}$$

and that inhomogeneous Equation (27) is satisfied, which is done by integrating over a small interval at $z = 0$:

$$C_1 H_\nu^{(1)'}\big(\lambda e^{hz_0/2}\big) - C_2 J'_\nu\big(\lambda e^{hz_0/2}\big) = 2/\big(h\lambda e^{hz_0/2}\big). \tag{29}$$

Recalling the Wronskian relationship $W_z[J_\nu(z), H_\nu^{(1)}(z)] = 2i/(\pi z)$, the solution for C_1 and C_2 is

$$C_1 = -i\pi J_\nu\big(\lambda e^{hz_0/2}\big)/h \qquad C_2 = -i\pi H_\nu^{(1)}\big(\lambda e^{hz_0/2}\big)/h. \tag{30}$$

$G_{\hat{A}}(x, y, z + z_0, z_0)$ is found by performing the inverse Fourier transforms, which in cylindrical coordinates are

$$G_{\hat{A}}(x, y, z + z_0, z_0) = \frac{1}{4\pi^2} \int_0^\infty \int_0^{2\pi} dk_\rho d\alpha k_\rho e^{ik_\rho \rho \cos(\phi - \alpha)} G_{\hat{A}}(k_\rho, \alpha, z + z_0, z_0) \tag{31}$$

$$= -\frac{i}{2h} \int_0^\infty dk_\rho k_\rho J_0(k_\rho \rho) J_\nu \Big[\lambda e^{h(z+z_0)/2} \mu(-z) + \lambda e^{hz_0/2} \mu(z)\Big] H_\nu^{(1)} \Big[\lambda e^{h(z+z_0)/2} \mu(z) + \lambda e^{hz_0/2} \mu(-z)\Big], \tag{32}$$

where $\mu(z)$ is the Heaviside step function. Therefore $G_{\hat{A}}(\mathbf{r}, z_0)$ is given by

$$G_{\hat{A}}(\mathbf{r}, z_0) = -\frac{i}{2h} \int_0^\infty dk_\rho k_\rho J_0(k_\rho \rho) J_\nu \Big[\lambda e^{hz/2} \mu(z_0 - z) + \lambda e^{hz_0/2} \mu(z - z_0)\Big] H_\nu^{(1)} \Big[\lambda e^{hz/2} \mu(z - z_0) + \lambda e^{hz_0/2} \mu(z_0 - z)\Big]. \tag{33}$$

We find $\mathbf{A}$ by integrating $G_{\hat{A}}(\mathbf{r}, z_0)$ over the source $-\mu_0 \hat{\mathbf{J}}_s$ and transforming $\hat{\mathbf{A}}$ to $\mathbf{A}$ using Equation (23).

5. Magnetoquasistatic Solution Example

We consider, as an analytically tractable example, the response to a current sheet

$$\mathbf{J}_s = \hat{\mathbf{x}} K \delta(z), \tag{34}$$

where K is a surface current density. The response for a component of $\hat{\mathbf{A}}$ is found as follows

$$\begin{aligned}
\hat{A} &= -\mu_0 \int_{-\infty}^{\infty}\int_{-\infty}^{\infty}\int_{-\infty}^{\infty} d\mathbf{r}_0 K\delta(z_0) G_{A'}(\mathbf{r}, z_0) && (35)\\
&= \frac{iK\mu_0}{2h}\int_0^{\infty}\int_0^{2\pi} d\rho\, d\phi\rho \int_0^{\infty} dk_\rho k_\rho J_0(k_\rho\rho) J_\nu\left[\lambda e^{hz/2}\mu(-z)+\lambda\mu(z)\right] H_\nu^{(1)}\left[\lambda e^{hz/2}\mu(z)+\lambda\mu(-z)\right] && (36)\\
&= \frac{i\pi K\mu_0}{h}\int_0^{\infty} dk_\rho \delta(k_\rho) J_\nu\left[\lambda e^{hz/2}\mu(-z)+\lambda\mu(z)\right] H_\nu^{(1)}\left[\lambda e^{hz/2}\mu(z)+\lambda\mu(-z)\right] && (37)\\
&= \frac{i\pi K\mu_0}{h} J_0\left[\lambda e^{hz/2}\mu(-z)+\lambda\mu(z)\right] H_0^{(1)}\left[\lambda e^{hz/2}\mu(z)+\lambda\mu(-z)\right]. && (38)
\end{aligned}$$

The x component of the conduction current $i\omega\boldsymbol{\sigma}\cdot\mathbf{A}$ is shown in Fig. 2. The upper cutoff of the conduction current distribution results from the exponential increase in magnetic diffusion time with altitude, and the lower cutoff arises from the exponential decrease in conductivity.

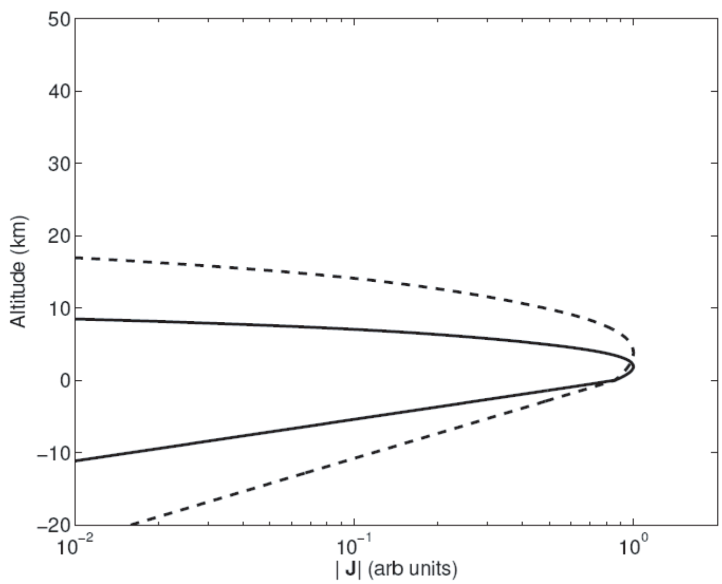

Figure 2: Magnetoquasistatic conduction current distributions. Solid line: $1/h = 2.5\,\text{km}$, $1/\sqrt{\omega\mu_0\sigma_p} = 100\,\text{km}$, $\sigma_P = \sigma_H$. Dashed line: $1/h = 5.0\,\text{km}$, $1/\sqrt{\omega\mu_0\sigma_p} = 100\,\text{km}$, $\sigma_P = \sigma_H$.

6. Conclusion

This work has determined the response of inhomogeneous, anisotropic media to conductivity perturbations in the static and magnetoquasistatic limits. The responses have been characterized as Green's functions, which can provide the response current distribution if the source currents are known a priori. Some simple source currents have been considered here. More discussion of ionospheric source currents can be found in [1].

REFERENCES

1. Stubbe, P. and H. Kopka, "Modulation of the polar electrojet by powerful HF waves," *Journal of Geophysical Research*, Vol. 82, 2319–2325, 1977.
2. Zhou, H. B., K. Papadopoulos, A. S. Sharma, and C. L. Chang, "Electronmagnetohydrodynamic response of a plasma to an external current pulse," *Physics of Plasmas*, Vol. 3, 1484–1494, 1996.

Surface and Volume Scattering from Rough Heterogeneous Media in the Optical Domain

H. Chanal, J. P. Segaud, and P. Borderies
ONERA Centre de Toulouse, France

M. Saillard
Université de Toulon et du Var, France

Scattering from rough heterogeneous media involves both surface and volume effects. This issue has many applications in geophysics, remote sensing (from the microwave domain to the optical one) and biomedicine, for instance. In optics, the total diffraction problem must be addressed accurately to understand the scattering properties of coatings. But volume and surface scatterings are both difficult issues that are usually studied separately. There is a need for rigorous methods that are able to handle in the same way both phenomena without any coupling hypothesis. We choose to use the Finite Difference Time Domain (FDTD) method as such a reference one. A Monte Carlo process is built to access to the statistical properties of rough heterogeneous media. It is composed of two steps:

- the generation of one deterministic medium realization;
- the FDTD computation over this realization to derive the electromagnetic near and far fields.

This process is repeated and the successive results are averaged to give the statistical response of the inhomogeneous medium. This work is restricted to the bidimensional geometry with the aim of investigating fine surface-volume coupling effects.

In a first part, we study the scattering of rough surfaces (homogeneous medium). Random profiles with gaussian height distributions and gaussian or exponential autocorrelation functions (ACF) are considered. Our method is compared with the Method of Moments (MoM) on a unique deterministic realization and on the average scattering patterns. The agreement proves to be always excellent for gaussian ACF and to decrease when the roughness increases for exponential ones due to the representations of the fine structures in the surface profiles which are different in both methods.

Then, we investigate the volume effects with randomly distributed cylindrical scatterers embedded in a semi-infinite homogeneous binder with flat interface. Effective propagation parameters are derived from the evolution of the near field with depth. These numerical results are compared to the Maxwell-Garnett and Bruggeman mixing laws and the Foldy-Twersky and Keller perturbative models for both polarization modes, validating the process implementation and allowing to precise the validity domain of approximate approaches.

Finally, we tackle the general case of rough heterogeneous media. Several interface types (the previous gaussian and exponential ACF surfaces and a new type of surfaces with profile correlated to the scatterers distribution in volume) are considered on top of heterogeneous media over a large range of volume fractions, particle sizes and optical constants. The hypothesis of surface and volume scattering splitting is systematically tested and surface -volume coupling effects are analyzed.

Optical Properties of Metal Nanoclusters on a Substrate

S. V. Sukhov
Institute of Radio Engineering and Electronics of RAS, Ulyanovsk Branch, Russia

S. G. Moiseev
Military Communications University, Ulyanovsk Branch, Russia

The past few years demonstated extended use of metallic nanoclusters as sensing elements in various biosensor systems. Most of these systems exploit the unique optical properties of gold nanoparticles determined by the localized surface plasmon resonance. The operation of such devices is based on the dependence of the plasmon resonance on either the local dielectric environment of an individual nanoparticle or the mean distance between the approaching particles. Reports are now available on the biospecific interactions taking place on gold particles in systems where nanoparticles are represented as ordered structures, either as selfassembled monolayers or as part of polymer assemblies. Urgency of study of properties of plane arrays of nanoparticles is related also with creation of covers with tunable optical properties. Varying the mutual arrangement of nanoparticles, one can change the reflective properties of surface and its resonant properties in wide spectral range.

We present a detailed discussion of optical properties of aggregated conjugate-based structures such as bispheres, linear chains, plane arrays. The interaction of electromagnetic wave with a cluster of nanoparticles situated on a substrate is considered. Our attention is focused on dependence of extinction and scattering spectra on the optical coupling of conjugates, effects of interparticle spacing and cluster structure. The reflection of light from nanoclusters is analyzed with structure factor taken into account for different mutual arrangement of nanoparticles. Both Coulomb (near-field) and retarded parts of optical fields acting between nanoparticles and from substrate side were considered in details.